Central European Geology, Vol. 60/1, 73–133 (2017)
DOI: 10.1556/24.60.2017.004

Collection of the thinnest: A unique eggshell assemblage from the Late Cretaceous vertebrate locality of Iharkút (Hungary)

Edina Prondvai[1,2]*, Gábor Botfalvai[2,3,4], Koen Stein[5], Zoltán Szentesi[4], Attila Ősi[2,4,6]

[1]Evolutionary Morphology of Vertebrates, Ghent University, Ghent, Belgium
[2]MTA-ELTE Lendület Dinosaur Research Group, Budapest, Hungary
[3]MTA-MTM-ELTE Research Group for Paleontology, Budapest, Hungary
[4]Department of Palaeontology and Geology, Hungarian Natural History Museum, Budapest, Hungary
[5]Earth System Science – AMGC, Vrije Universiteit Brussel, Brussels, Belgium
[6]Department of Paleontology, Eötvös Loránd University, Budapest, Hungary

Received: June 2, 2016; accepted: October 6, 2016

As a result of several years of screen-washing activity, a remarkable assemblage of eggshell fragments has been recovered from the Late Cretaceous vertebrate locality of Iharkút, Hungary. Detailed investigation of the assemblage by multiple visualization techniques (scanning electron microscopy, polarizing light microscopy, X-ray micro-computed tomography), quantitative morphometric analyses, and micro X-ray fluorescence spectrometry revealed a diverse composition of five different eggshell morphotypes (*MT I–MT V*) and three subcategories within the second morphotype (*MT II/a*, *b*, *c*), with *MT I* being by far the most abundant (83%) in the assemblage. *MT I*, *MT III*, and *MT V* represent theropod dinosaurian eggshells, whereas *MT II* and *MT IV* show characteristics of crocodilian and squamate eggshells, respectively. Hence, despite their fragmentary nature, these eggshells represent the first clear evidence that various sauropsid taxa had nesting sites near the ancient fluvial system of Iharkút. Besides the implied taxonomic diversity, two unique features add to the significance of this eggshell assemblage. First, it contains the thinnest rigid crocodilian (*MT II/c*) and squamate (*MT IV*) eggshells ever reported. Moreover, one of the identified theropod morphotypes, *MT I*, is also among the thinnest fossil dinosaurian eggshells, the thinness of which is only rivalled by the eggshells of the smallest Mesozoic avian eggs known to date. Second, the Iharkút eggshell assemblage consists exclusively of thin eggshells (≤300 μm), a condition unknown from any other fossil eggshell assemblages described to date. Combined with the knowledge acquired from skeletal remains, these peculiarities give additional insights into the paleoecology of the terrestrial sauropsid fauna once inhabiting the ancient island of Iharkút. Finally, the presence of well-preserved eggshells recovered from two different sites representing different depositional environments provides further evidence for previous taphonomic and sedimentological conclusions, and also expands our knowledge of the special conditions that allowed the preservation of these delicate eggshell fragments.

Keywords: eggshell assemblage, Iharkút, Late Cretaceous, dinosaurian and crocodilian eggshells, thin sections, SEM

*Corresponding author: Edina Prondvai; Evolutionary Morphology of Vertebrates, Ghent University, Ledeganckstraat 35, 9000 Gent, Belgium
E-mails: edina.prondvai@gmail.com; edina.prondvai@UGent.be

ISSN 1788-2281

Introduction

The exceptional Santonian beds of the Upper Cretaceous Csehbánya Formation at the Iharkút vertebrate locality (Bakony Mountains, northwestern Hungary) have yielded a rich and diverse assemblage of vertebrate and plant remains during the last 15 years of excavations (Ősi et al. 2012a; Csiki-Sava et al. 2015), in which traditional collecting techniques were augmented by screen-washing of the most productive, bone-bearing layers. In addition to the diverse plant material (Bodor and Baranyi 2012; Bodor et al. 2012) and microvertebrate remains, thousands of eggshell fragments were also recovered from the screen-washed sediments. Even though minute in size ($\leq$3 mm $\times$ 5 mm), these eggshell fragments represent the first evidence of nesting activity of amniotes with hard-shelled eggs in this area. By applying diverse visualization techniques and quantitative methods, here we give a detailed description of the eggshells with the aim of relating them to presumptive egg-laying taxa and discuss the most probable taphonomic conditions that allowed the preservation of such fine structures in two different depositional environments.

Geological background and depositional environment

The investigated stratigraphic unit of the Csehbánya Formation, which had been exposed by open-pit bauxite mining activity in the area of Iharkút (Fig. 1A), is made up of a cyclic alternation of sandstone and variegated siltstone and clay layers with sporadic intercalation of thin coal seams. This sedimentological setting implies that the exposed layers were deposited by an anastomosing fluvial system in a topographically low-level, wet, alluvial plain environment (Botfalvai et al. 2016). The floral assemblage (subtropical floodplain forest vegetation), the absence of desiccation cracks, the common presence of hydromorphic paleosols, and the subordinate amount of secondary (pedogenic) carbonate accumulation indicate that the climate was predominantly humid but seasonal, with flash-flood-like episodes (Botfalvai et al. 2015, 2016). Palynological data imply a Late Santonian age for this sequence (Bodor and Baranyi 2012).

The Iharkút open-pit bauxite mine contains several fossiliferous sites representing different stratigraphic levels within the Csehbánya Formation. Among these, the most productive SZ-6 site is situated in the southern part of the open pit with an extension of ca. 5,000 m^2. The most extensively and thoroughly investigated basal strata of site SZ-6 (hereafter referred to as Unit 1; Fig. 1B), which yielded the most abundant vertebrate remains, including eggshell fragments, is represented by a 10–50-cm-thick basal breccia layer composed of gray-green sand, siltstone, clay clasts, and pebbles. The poorly sorted sandy breccia is interrupted by laminated siltstone horizons; these coarse- and fine-grained layers are repeated several times resulting in a stacked fining-upward series of units. The coarser part of Unit 1 suggests a flash-flood sequence deposition, which started with a high flow regime

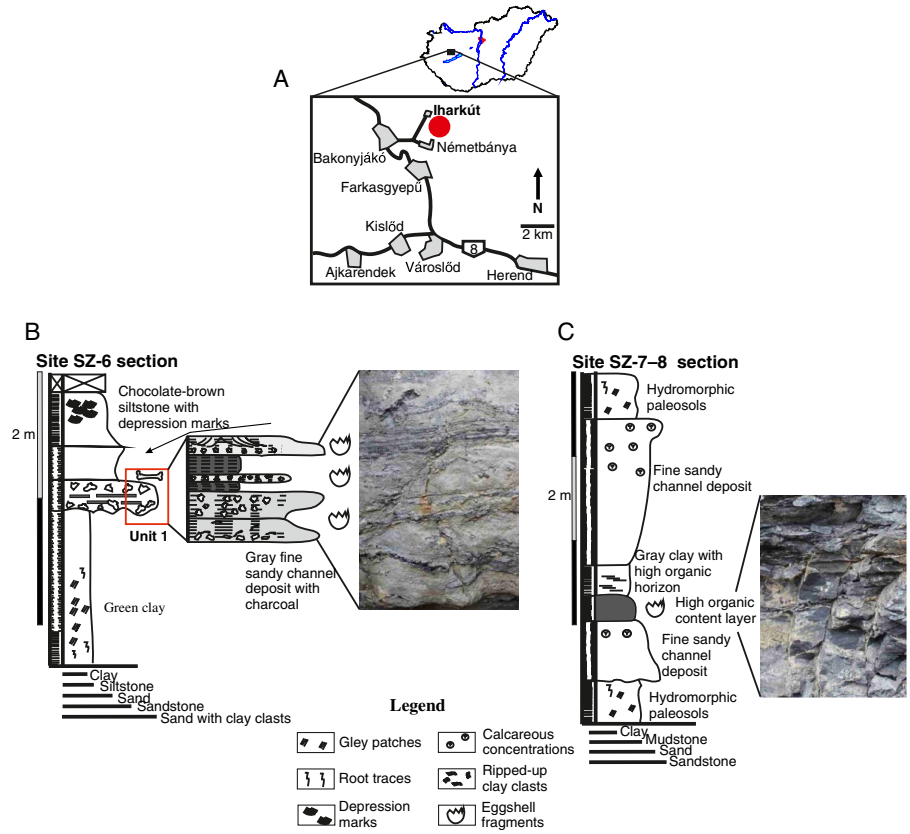

Fig. 1
Map and schematic stratigraphic sections of the two sites yielding eggshell fragments. (A) Location map of the Iharkút vertebrate locality. Schematic stratigraphic section of site SZ-6, Unit 1 (B) and SZ-7–8 (C) highlighting the eggshell-rich layers

characterized by sandstone and clay clasts, whereas the siltstone layers are indicative of waning flow velocity and deposition from suspension in standing water, following the minor flow pulse. Along with its taphonomic characteristics, this sedimentology suggests that Unit 1 was deposited by ephemeral high-density flash-flood events probably triggered by episodic heavy rainfalls. It acted as a trap where current velocity suddenly decreased and the poorly sorted sand, ripped-up clay clasts, pebbles, bones, and eggshell fragments accumulated (Botfalvai et al. 2015, 2016).

The screen-washed layers of the other site, SZ-7–8 (Fig. 1C), which to date yielded only microfossils (including eggshell fragments), are composed of 10- to 20-cm-thick, dark gray silt, and clay beds enriched in coalified plant material and amber. The

depositional area of this site was part of the low-level (poorly drained) floodplain with elevated water table characterized by overall hydromorphy; the dark sandy siltstone was deposited in small-scale stagnant (poorly oxygenated) pools of the floodplain (Botfalvai et al. 2015, 2016).

Materials and analytical methods

The excavation methods and circumstances and the sedimentological characteristics of the Iharkút locality (Botfalvai et al. 2016) usually prevent the *in situ* recognition, separation, and collection of very small and fragile fossils. Therefore, despite its destructive aspects (e.g., intensive fragmentation resulting in significant size reduction), only screen-washing could reveal the presence of the thin (50–350 μm) eggshell fragments from two different sites, SZ-6 (Unit 1) and SZ-7–8. These eggshells were extracted from the coarse-grained fraction (1–5 mm) of the residue (~48 kg from SZ-6 and ~2 kg from SZ-7–8) under stereo microscope (Motic, SMZ-140). Due to the small size, extremely fragile nature, and thinness of the eggshell fragments, complete removal of sediment from the depressions and pits of their surface was not always possible.

Based on gross morphology, eggshells were categorized into different morphotypes. Relative abundances of the different morphotypes were quantified as their percentage contribution to the total weight of the eggshell assemblage (w/w %). To reveal the identity of the egg-laying taxa, fine structural characteristics of the eggshells with the least attached sediment were investigated in well-preserved morphotype representatives under scanning electron microscope (SEM, Hitachi S-2600N at 20 kV from 5–8 mm distance), in X-ray micro-computed tomography (μCT, phoenix v|tome|x m), and as thin sections under polarized light microscope (PLM, Nikon ECLIPSE LV100 POL). Fragments used for SEM imaging were coated with gold–palladium using an XC7620 Mini Sputter Coater. Thin sections were photographed with QImaging MP5.0 digital microscope camera and the pictures initially processed with Image-Pro Insight 8.0 software. For testing whether different eggshell morphotypes can be quantitatively distinguished as well, structural features were measured on SEM and PLM images with the ImageJ free image processing program and used for comparative analysis. Pore densities were calculated based on μCT images. Due to the screen-washing and the fragmentary nature of the eggshells, it was impossible to ensure the independent origin of the individual fragments in the statistical evaluation of the measured characters. Therefore, multiple measurements were taken of each variable along the length of every thin section, and several different data sets were created for the different analyses to explore and analyze intra- and inter-specimen variation of the quantified microstructural characters within and between different morphotypes. Table 1 specifies the measured variables and the methods they were used in, whereas Fig. 2 demonstrates how the measurements in thin sections were performed.

Table 1
Morphometric variables taken from SEM, thin section, and μCT images for qualitative and quantitative analyses. The abbreviations of the variables used in further tables and figures and the methods in which they were used are indicated

Variable	Abbreviation	Method
Thickness without ornamentation (=total thickness, μm)	Th	Uni- and bivariate analyses
Thickness with ornamentation (μm)	OTh	Uni- and bivariate analyses
Mammilla width (μm)	MW	Uni-, bi-, and multivariate analyses
Mammillary layer thickness (μm)	MTh	Uni-, bi-, and multivariate analyses
Palisade/second layer thickness (μm)	PTh	Uni-, bi-, and multivariate analyses
External layer thickness (μm)	ETh	Uni- and bivariate analyses
Prism/eggshell unit width (μm)	PW/UW	Uni-, bi-, and multivariate analyses
Pore diameter (μm)	PØ	Qualitative comparison
Pore density (nr/mm^2)	PD	Qualitative comparison
Cavity density (nr/mm^2)	CD	Qualitative comparison
Eggshell unit angle (°)	SUA	Uni-, bi-, and multivariate analyses in *MT II* subcategories

All quantitative analyses were performed using R Gui (64-bit) free statistical software. After initial univariate exploration of data structure, bivariate non-parametric permutation tests from R packages "coin" (function "oneway_test"; Hothorn et al. 2015), "exactRankTests" (function "perm.test"; Hothorn and Hornik 2015) and "perm" (function "permTS"; Fay 2010), and multivariate methods, such as principal component analysis (PCA, function "prcomp") based on covariance matrix, non-metric multidimensional scaling (NMDS, function "monoMDS") from package "vegan" (Minchin and Oksanen 2015), agglomerative hierarchical cluster analysis with *p* values acquired by multiscale bootstrap resampling (function "pvclust") from package "pvclust" (Suzuki and Shimodaira 2014) were performed for deeper understanding of the microstructural diversity of the eggshell morphotypes. The significance level of the tests was set at $\alpha = 0.05$. Benjamini–Hochberg *p*-value correction was applied after multiple pairwise comparisons.

To explore whether different eggshell morphotypes show distinct chemical composition due to potential differences in taphonomic history, burial conditions, or

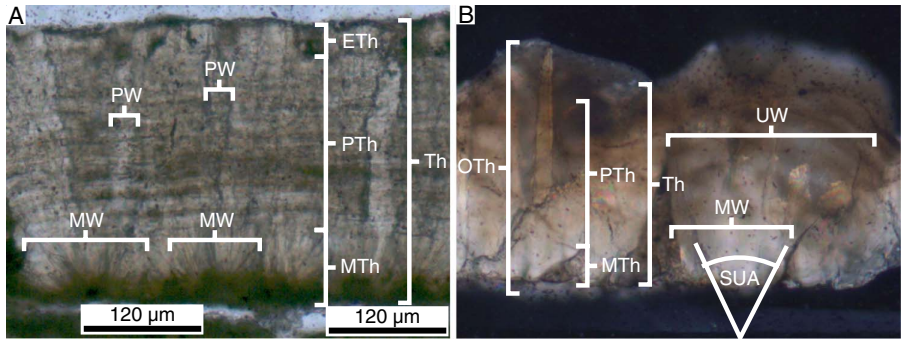

Fig. 2
Measurements of structural variables in thin section demonstrated in two substantially different eggshell morphotypes. For explanation of variable abbreviations, see Table 1

diagenesis, element composition and distribution in the eggshell fragments were investigated with an M4 Tornado (Bruker Nanotechnologies, Berlin, Germany) tabletop micro X-ray fluorescence spectrometer (µXRF) to infer possible compositional differences between different eggshell types. The fossils were scanned under high vacuum with a Rhodium X-ray tube (anode settings 50 kV, 600 µA, no filter, with three to four cycles of 20 ms per pixel and a spot size of 25 µm). Cross sections were scanned from epoxy resin-embedded radially cut eggshell specimens, whereas additional internal and external surfaces were scanned from non-stabilized specimens. Line scans were extracted from the surface maps of radially cut specimens to reveal potential differences in element concentrations from inner to outer eggshell surface. Major chemical components of the fragments were interpreted and, in the case of crosscut specimens, quantified from deconvolution spectra of the element distribution maps using the interactive oxide quantification method in the Bruker M4 software. Quantified results of net photon counts were standardized to those for Rh (anode material) and exported to a spreadsheet for multivariate (PCA in R) analysis to reveal any potential groups of specimens based on differences in composition.

In this study, we do not apply ootaxonomic classification but rather restrict our considerations to the morphological description, data analysis, and comparison of microstructural features of our specimens with those of other known extant and fossil eggshells.

The studied eggshell assemblage and their thin sections are housed in the Hungarian Natural History Museum (MTM, Budapest, Hungary). Because eggshell pieces belonging to the same category were frequently fragmented further by handling, and because several fragments could have belonged to the same egg specimen, the thousands of individual fragments were not given individual specimen numbers. Instead, the eggshell fragments are categorized, kept in separate holders along with

their thin sections, and cataloged by the five identified morphotypes under the following inventory numbers: Morphotype I (*MT I*): MTM VER 2015.336; Morphotype IIa, b (*MT II/a*, *MT II/b*): MTM VER 2015.337.1; Morphotype IIc (*MT II/c*): MTM VER 2015.337.2; Morphotype III (*MT III*): MTM VER 2015.338; Morphotype IV (*MT IV*): MTM VER 2015.339; Morphotype V (*MT V*): MTM VER 2015.340. Hereafter, all investigated and demonstrated fragments will be referred to only by their corresponding morphotype groups, *MT I–MT V*.

Results

Whereas more than 2,000 eggshell fragments were recovered from 48 kg of coarse-grained sediment from Unit 1 of SZ-6, only five fragments were found in 2 kg of residue of the screen-washed layers of SZ-7–8. The total weight of the eggshell assemblage added up to 6.2–6.3 g. Twelve percent of the fragments could not be categorized into any morphotypes because their surface was either strongly eroded or encrusted by sediment and mineral crystals. The classifiable eggshell fragments were largely well preserved with distinct ornamentation and microstructural characteristics. They occasionally show different degrees of mechanical and/or chemical surface erosion and densely spaced pits and pinholes of variable sizes which seem to be traces of acidic erosion caused by bacterial activity (Smith and Hayward 2010) and/or by the inorganic chemical environment (Bravo et al. 2003; Clayburn et al. 2004). Based on gross morphology, more than 99% of the classifiable eggshell fragments could be grouped into three different morphotypes with very different relative abundances and a considerable diversity in ornamentation within two of the three groups (Fig. 3). Three other, very rare morphotypes (represented by only 1–5 fragments each), were also present in the assemblage and are described separately. Only morphotypes represented by five or more specimens were used in comparative quantitative analyses. Table 2 contains the mean and standard deviation values for each measured eggshell character.

Morphological descriptions

Morphotype I (MT I)

The most abundant morphotype, *MT I*, comprises 83% of the total weight of classifiable eggshells, with the few fragments recovered from SZ-7–8 all belonging to this type. *MT I* shows variably spaced tiny nodes (Ø: ~50–150 μm) and larger rings or crater-like ornamentation (Ø: ~100–200 μm) on the outer surface (Figs 3B–F and 4A–H). In some specimens, the nodes merge into a meshwork, whereas in others, they form confluent low ridges oriented in a preferred direction. The inner eggshell surface appears largely smooth or finely dotted under stereo microscope (Fig. 3A); however,

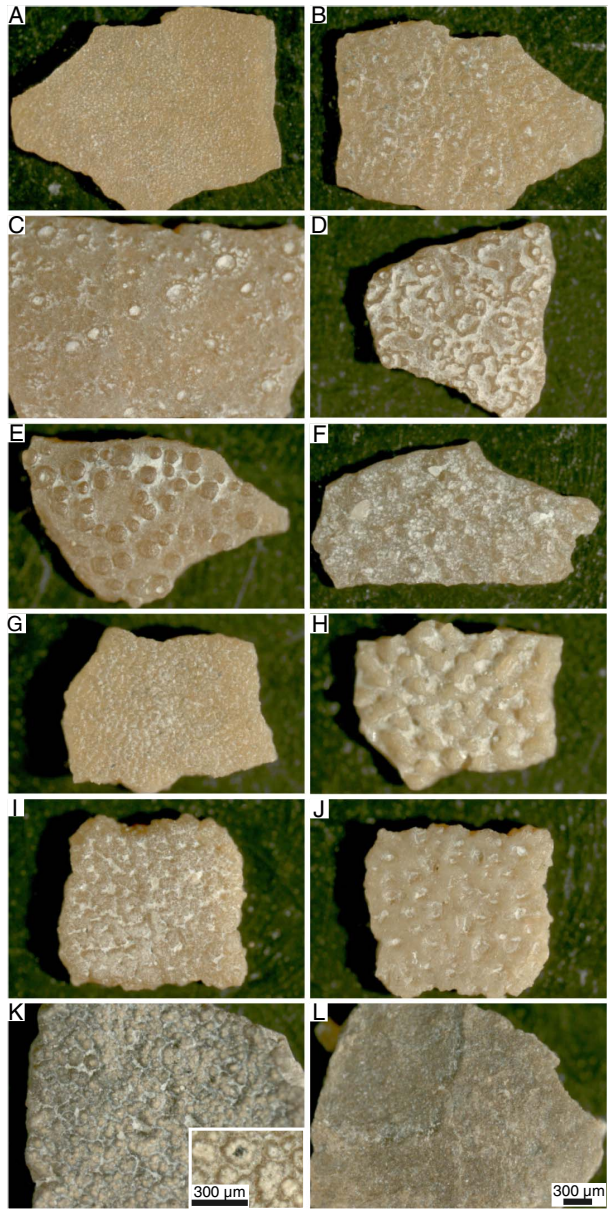

Fig. 3
The three different and most abundant morphotypes found in the Iharkút eggshell assemblage. (A–F) *MT I*, (G) and (H) *MT II/a*, (I) and (J) *MT II/b*, (K) and (L) *MT III*. (A), (G), (I), and (K) show the inner, (B–F), (H), (J), and (L) the outer eggshell surface of the respective morphotypes. Note the considerable diversity in surface ornamentation of *MT I* (B–F), and the robust mammillary aggregations in *MT III* [inset in (K)]. All images are at the same scale as (L), except the close-up inset in (K)

Table 2
Mean and corresponding standard deviation (SD) values of different morphometric variables calculated with pooled specimen data in each morphotype (MT). *MT II* here includes specimens from both subcategories *MT IIa* and *IIb*

MT	Th	OTh	MW	MTh	PTh	ETh	PW/ UW	PØ	PD	CD
MT I mean	150.69	192.20	12.62	17.59	123.72	17.91	19.49	23.4	2.7	2.7
MT I SD	13.32	14.62	4.27	5.48	13.15	3.20	5.54	3.7	–	–
MT II mean	208.34	292.63	64.40	37.94	158.79	–	151.20	22.6	2.9	15.4
MT II SD	29.68	50.12	38.31	9.76	26.46	–	39.22	2.2	–	–
MT III mean	261.32	–	88.79	60.82	189.62	29.11	25.57	27.2	0.7	3.8
MT III SD	55.04	–	42.24	19.02	37.35	5.67	8.47	7.7	–	–

the strongly cratered or flattened remnants of mammillary cones and the eggshell units delineated by the intermammillary grooves (e.g., Österström et al. 2013) are recognizable in the least eroded specimens under SEM (Fig. 4L–O). The average thickness of the intact shell in areas that lack ornamentation is ~130–160 μm, whereas the ornamentation increases the eggshell thickness to ~180–200 μm. Its general microstructure could be described as "dinosauroid-prismatic" (*sensu* Hirsch and Quinn 1990) with two to possibly three different structural layers: (1) thin mammillary layer (ML ~18 μm) with narrow (~13 μm) and very densely spaced mammillary cones (Fig. 5G–I, K); (2) palisade layer (PL ~124 μm) with thin (~19 μm) vertical prisms (Fig. 5B, C, J); and (3) potentially a thin external layer (EL ~18 μm) that is distinguishable in a few fragments in SEM images (Fig. 4J, K). Hence, the thickness ratio among the three layers can be given as ML:PL:EL = 1:7:1. The crater-like concavities in the apical part of the mammillae (Figs 4L and 5E, H, I) most likely represent embryonic resorption craters (Jenkins 1975; Board and Sparks 1991) indicating either a late embryonic developmental stage or post-hatching state of the original egg (Kundrát et al. 2008; Agnolin et al. 2012; Österström et al. 2013). Fine ultrastructural characteristics of mammillae, such as spherulites, are difficult to discern; however, some specimens show platelet-like crystals radiating from the cratered apex and occasionally showing darker coloration (Fig. 5H, I) that may indicate an originally higher organic content around the former organic core (Fig. 4M, N). There is a gradual transition between the mammillary and the prismatic PLs (Fig. 5G, H). The individual prisms seem to flare underneath the nodes (Figs 4I and 5F, G). Horizontal accretion lines or laminations (tabular structure) are visible throughout the PL in thin section (Fig. 5) and in some specimens under SEM, as well (Fig. 4F). The EL appears to comprise vertical crystals (Fig. 4J); however, it may also represent a diagenetically altered layer of calcite as shown in other fossil

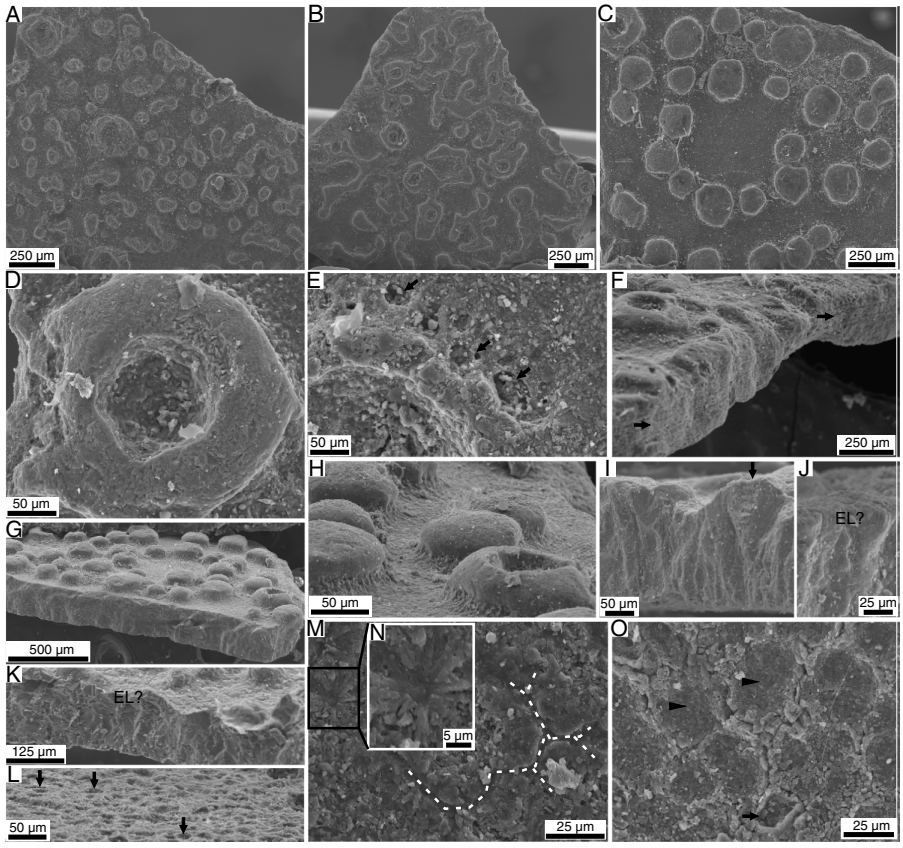

Fig. 4
SEM images of fragments belonging to *MT I*. (A–E) Outer surface morphology of *MT I* showing high diversity in density, arrangement, and relative proportion of nodes, more confluent ridges, and ring- or crater-like ornamentation. Erosion craters around the ornamentation ring [black arrows in (E)] may have resulted from bacterial activity. (F, G) Oblique view on the outer surface and broken edge and (H) close-up from the same view as (G) showing details of node morphology. Tabular structure appears on the eroded surface of the broken edge in (F) as fine horizontal lines (black arrows). (I) Radial view on the freshly broken surface revealing slender prisms and flaring crystals at the nodes (black arrow). (J, K) A putative external layer with vertical crystal blocks (EL) seems to be present on the radial broken surface of some fragments. (L) Oblique view on the inner eggshell surface showing craters in former mammillary cones (black arrows) resulting from embryonic resorption. (M, N) Inner eggshell surface with a rare instance of possibly preserved mammillary cone magnified in (N) and a network of intermammillary grooves (white dashed line) delineating the eggshell units. Note the rosette-like radiating crystals organized around a circular empty pit where the original organic core of the mammilla may have been located in (N). (O) Eggshell units (black arrowheads) as they appear on the inner surface where no mammillary processes have been preserved and the opening of a pneumatic canal (black arrow) in between the units exhibiting thickened margins

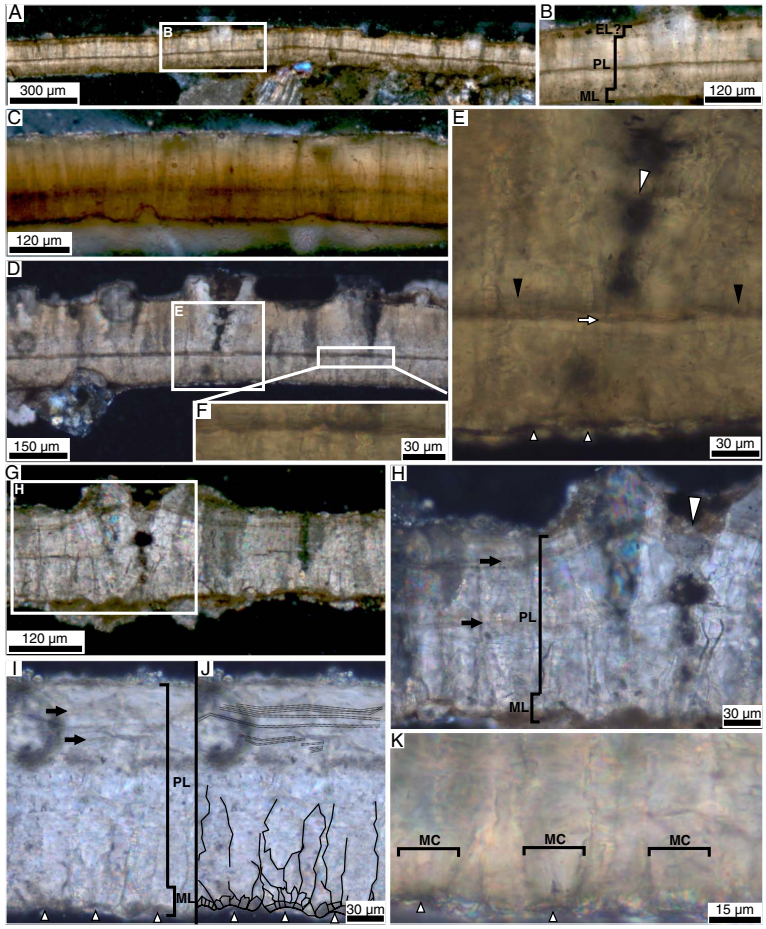

Fig. 5
Radial thin sections of *MT I* specimens. Diverse microstructural appearance represented by five different fragments of *MT I*, (A, B), (C), (D–F), (G–J), and (K), is due to differences in preservation and in the thickness of the thin sections. The "dinosauroid-prismatic" microstructure is characterized by long, narrow prisms (A–C), small, conical mammillae (I–K), and a tabular structure with horizontal accretion lines in the prismatic layer (H–J). The apices of mammillae are mostly worn or cratered by erosion and/or embryonic resorption [white short arrowheads in (E) and (I–K)]. Note the narrow, converging edges of mammillary cones (MC in K) and the darker coloration of platelet-like crystals at their mostly cratered, apical region in (H) and (I) [(I) same as (H) overlain by interpretative line drawing]. Tabular structure appears as fine lamination or darker lines [black arrows in (H) and (I), fine dotted lines in (J)]. Pores are usually funnel-shaped and open through the nodes [(D, E, G, H) marked by white long arrowhead in (E) and (H)] creating the crater-like ornamentation on the outer surface. Columnar extinction pattern is evident in thinner sections (G). Possible double-layer pathology was observed in an unusually thick fragment (D–F) exhibiting a well-defined discontinuity line with almost fibrous appearance (F) in the prismatic layer on top of which structures resembling newly formed mammillary cones occur [black arrowheads in (E)]. This discontinuity line seems to truncate a pore running from the outer surface but apparently terminating blindly at the line [white arrow in (E)]. Abbreviations: EL: possible external layer; PL: prismatic layer; ML: mammillary layer

eggshells (Antunes et al. 1998; Riberio et al. 2013). Under crossed plane polarizers, a strong columnar calcite-like extinction pattern is characteristic throughout the eggshell thickness (Fig. 5F, G).

The pore pattern of the pneumatic system is angusti- to obliquicanaliculate, composed of mainly vertically or slightly obliquely running pores, most of which exhibit a funnel shape where they open onto the outer surface through the crater-like ornaments (Figs 5D–G and 6A). Individual pores, defined as canals traversing the entire eggshell thickness, have an average diameter of ~23 μm (i.e., ~10%–15% of total eggshell thickness) with an average density of ~2.7/mm^2 (Fig. 7A). Anastomosing pore canals could not be observed; however, smaller, round pneumatic cavities within the PL and canals opening on the inner surface but blindly ending in the middle of the PL are as abundant as the pores piercing through the entire eggshell (Figs 6A and 7A). Similar

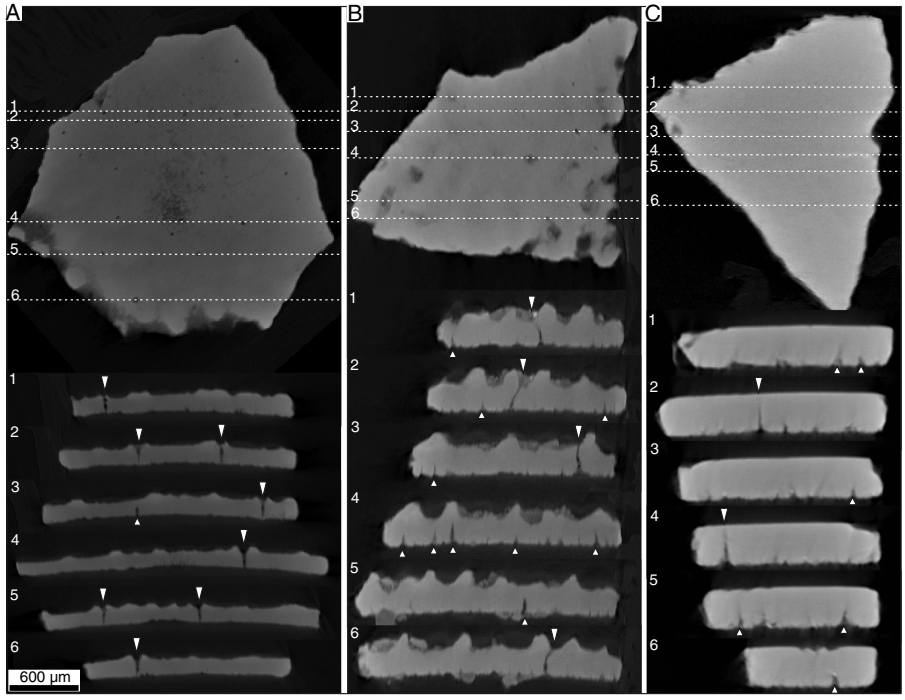

Fig. 6
μCT images of the three different morphotypes revealing pore shapes in radial virtual slices. The position of the planes of virtual cuts in (A) *MT I*, (B) *MT II/a*, and (C) *MT III* is indicated in mid-tangential sections (numbered white dashed lines) above and the corresponding radial serial sections are seen below. Note the different morphology and density of the pneumatic channel system with blindly ending cavities (short white arrowheads) and pores piercing through the entire eggshell thickness (white arrowheads) in the three different morphotypes

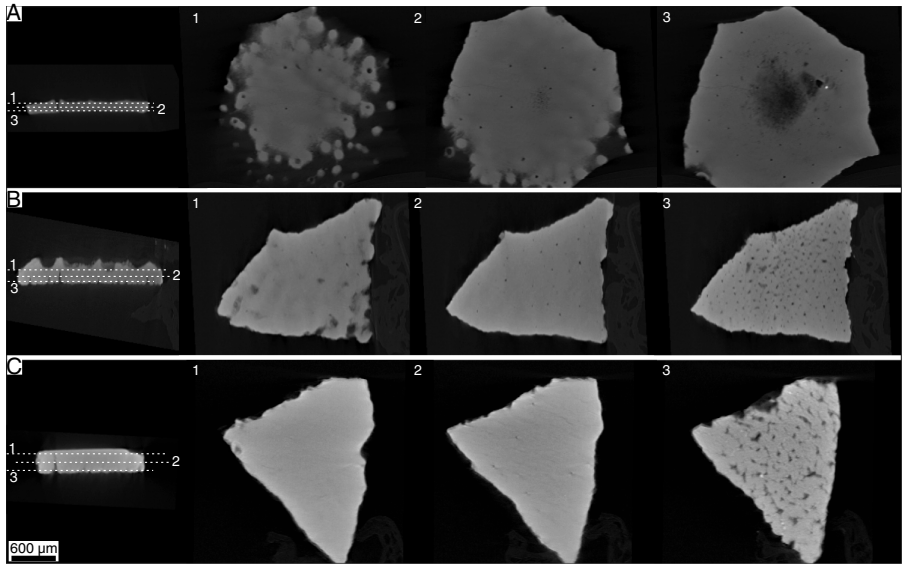

Fig. 7
µCT images of the three different morphotypes showing pore densities in tangential virtual slices. The position of the three planes of virtual cuts in (A) *MT I*, (B) *MT II/a*, and (C) *MT III* is demonstrated in radial virtual slices (numbered white dashed lines) on the left, and the resulting tangential serial sections are shown on the right. Plane 1, 2, and 3 represent tangential cutting planes close to the outer surface, in the mid-level of the palisade layer, and at the upper border of the mammillary layer, respectively. Note the increase in pneumatic canal density toward the mammillary layer in each specimen

blind canals have also been observed and described as "incomplete pore canals" in chicken eggshells (Riley et al. 2014). In a few specimens, particular pores were surrounded by a pronounced, ring-like thickening on the inner surface of the eggshell (Fig. 4O).

A single thin-sectioned specimen seems to show double-layered pathology (Fig. 5D, E), as also demonstrated in amniotes laying hard-shelled eggs, such as turtles, some birds, and other dinosaurs (Ewert et al. 1984; Zelenitsky and Hills 1997; Jackson and Varricchio 2003; Hayes 2005). This fragment shows two superimposed eggshell layers separated by a distinct line that has a fibrous appearance and may represent remnants of the intercalated shell membrane between the two layers. Above this line, the basis of the upper layer regionally reveals a second row of mammillary cones (Fig. 5E). Furthermore, the single pore revealed in the thin section appears to have formed only in the outer layer because it does not seem to extend through the inner, much thinner eggshell layer (Fig. 5D, E). These microstructural features have been described as reliable characteristics to recognize double-layer eggshell pathologies in fossils (Jackson and Schmitt 2008). This specimen is also significantly thicker (~200 µm) than the other fragments

belonging to this morphotype (~150 μm), possibly due to the double-layered pathologic condition. Nevertheless, cathodoluminescence and electron backscatter diffraction methods have recently been considered the most reliable methods to differentiate whether double-layered eggshells are of biological (pathological) origin or result from taphonomic and diagenetic recrystallization events (Moreno-Azanza et al. 2016).

Based on its microstructural characteristics, *MT I* represents a dinosaurian eggshell.

Morphotype II (MT II)

On the basis of the initial stereo microscopic investigation, the second most abundant form (15%) in the classifiable assemblage of eggshell fragments, *MT II*, was first identified as a homogeneous group (Fig. 3G–J) with the observation that the surface ornamentation is often highly eroded in several specimens (Fig. 3J). However, most specimens showing the originally presumed strong erosion on the outer surface have a very rough inner surface due to the presence of pronounced, robust mammillary knobs (Fig. 3I). An erosion pattern of such asymmetry is unlikely because mechanical and chemical abrasion are expected to affect both sides of the eggshells to some extent (Bravo et al. 2003; Clayburn et al. 2004; Smith and Hayward 2010), whereas embryonic resorption would have acted more on the inner than the outer eggshell surface (Jenkins 1975; Board and Sparks 1991; Österström et al. 2013). Therefore, the strongly reduced ornamentation observed in specimens with pronounced mammillary knobs is more likely to be a genuine character rather than representing mechanical erosion or incubation-induced degradation (Ferguson 1982). SEM and PLM inspection supported this hypothesis by showing that *MT II* is composed of two different subcategories (Figs 8 and 9). *MT II/a* is typified by specimens possessing pronounced ridges and tubercles on their outer surface (Figs 8A, C, and 9A), which may be described as sageno- or ramotuberculate ornamentation (*sensu* Mikhailov 1991). *MT II/b* is represented by specimens showing lower elevations and shallower pits on their outer surface (Figs 8B, D, and 9B) than specimens of *MT II/a*. In *MT II/a*, the thickness of the ornament tubercles may exceed 50% of the non-ornamented eggshell thickness (~200–240 μm) but usually remains between 30% and 40% of the latter (Figs 8E and 9A). By contrast, surface sculpture of *MT II/b* reveals itself only as a slight irregularity of the outer surface with an overall eggshell thickness range of ~190–220 μm (Figs 8D, F, and 9B, D). Nevertheless, different degrees of surface erosion of mechanical and/or incubation-induced origin, including embryological resorption, occurring both *II/a* and *II/b*.

Both subcategories share wedge-shaped eggshell units with robust mammillary cones which lack the radial crystal organization (Figs 8I, J, and 9) that characterizes dinosaurian and chelonian mammillae (Hirsch 1989; Mikhailov 1997; Moreno-Azanza et al. 2014). Besides the presence or absence of surface sculpture, which may or may not be eroded, *MT II* specimens can be grouped into two subcategories based on quantified microstructural characters (see the Quantitative analyses section).

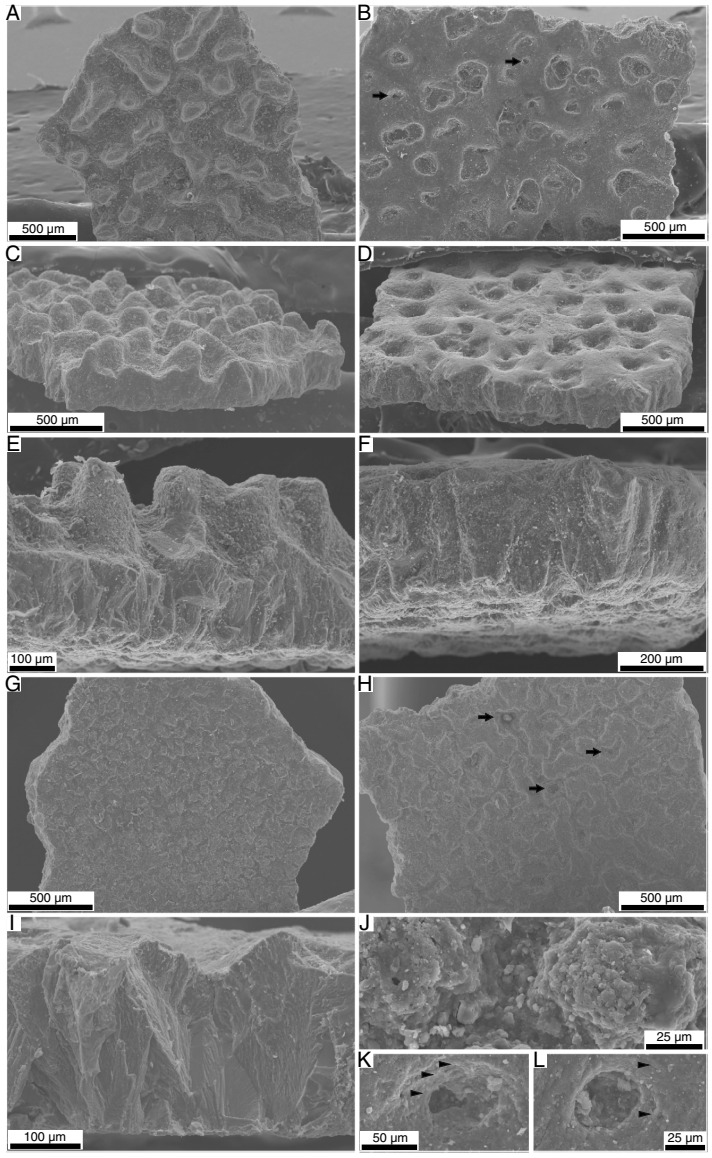

Fig. 8
SEM images of *MT II/a* and *II/b* specimens. (A–D) Sculptured outer surface in (A, B) straight and (C, D) oblique views, (E, F) broken surface in radial view, and (G, H) inner surface in straight view. (A), (C), (E), (G), and (B), (D), (F), (H) feature the same *II/a* and *II/b* fragments, respectively. Differences in surface sculpture are obvious with *II/a* exhibiting pronounced tubercles, free standing or merging to high ridges (A, C, F), and *II/b* showing low undulations interrupted by shallow pits on its outer surface (B, D, F). Both types share wedge-shaped eggshell units (E, F, I) and well-defined mammillary knobs (G, H, J). A few pore openings on the outer surface [black arrows in (B) and (H)] reveal faint stepped concentric rings [black arrowheads in (K) and (L)] likely representing erosion craters reported in crocodilian eggshells

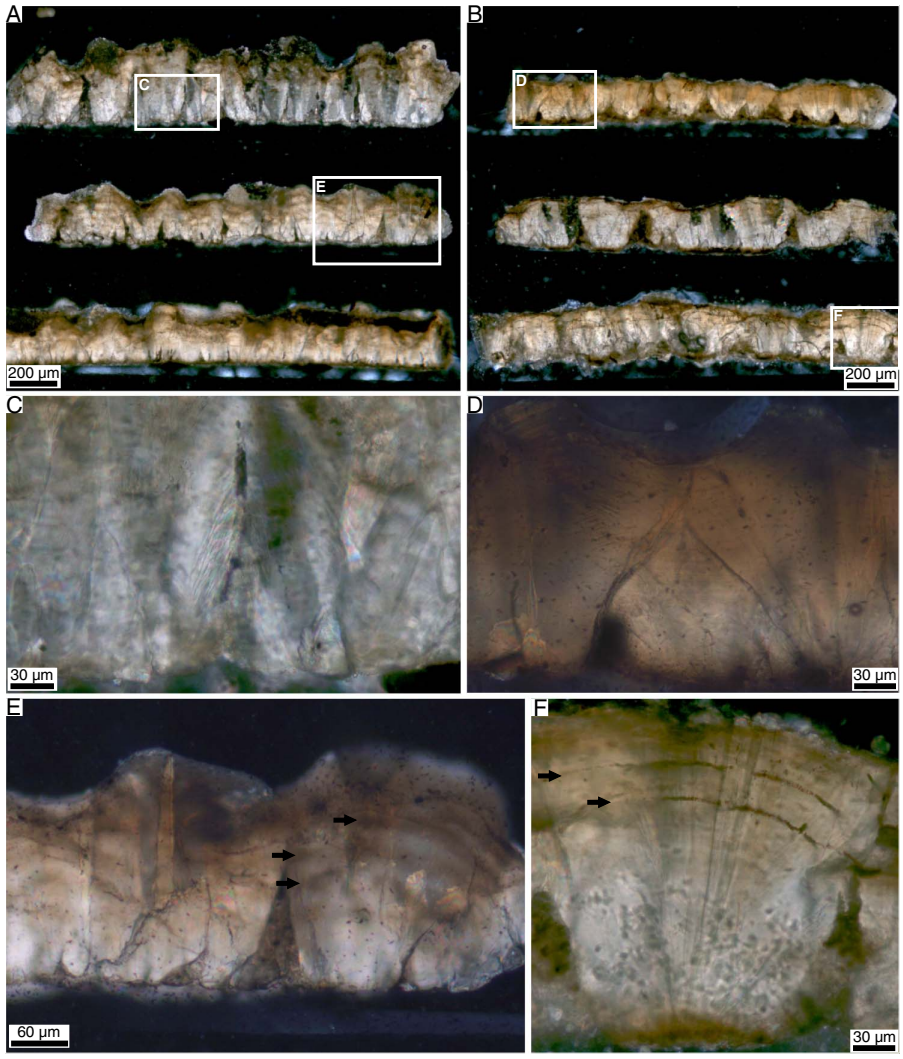

Fig. 9
Thin section images contrasting structural features of the two subcategories of *MT II*. (A, B) Overall microstructure and (C–F) eggshell unit morphology in *II/a* and *II/b*. *II/a* shows prominent protuberances on its outer surface (A), narrower eggshell unit wedges (A, C), and growth marks in form of dark bands (black arrows in E) undulating with the outer sculpture (A). *II/b* exhibits slight undulation as ornamentation (B), eggshell units of higher width to height ratio (B, D), and finer arching lines for growth marks (black arrows in F)

In thin section, the wedges show growth marks in both subcategories: in *II/a*, they are expressed in the form of broader and darker bands undulating with the surface sculpture (Fig. 9A, E), and in *II/b*, as accretion lines following the convex outline of

the eggshell units (Fig. 9B, F). However, none of these lines or any other sign of a tabular ultrastructure could be observed in SEM images.

The pneumatic system that was investigated in detail by μCT only in *MT II/a* is largely determined by the eggshell unit morphology. It can be characterized by a higher density (~13.7/mm^2) of blindly ending cone-shaped cavities enclosed by the converging edges of the wedge-shaped eggshell units and a lower density of angusticanaliculate pores (~2.6/mm^2) that extend through the entire eggshell (Figs 6B and 7B). These pores also originate from the intermammillary air spaces and exhibit an inverted funnel shape with a gradually tapering canal toward the outer surface. They run obliquely, mostly following the edges of the wedge-shaped shell units (Fig. 6B). The diameter of the tapering pore canal at the mid-level of the wedges averages around ~22 μm or ~10% of total eggshell thickness. No anastomoses between pneumatic canals have been observed. Some pore openings on the outer surface reveal faint stepped concentric rings (Fig. 8K, L), most probably representing erosion craters as reported in crocodilian eggshells (Ferguson 1982; Hirsch 1985; Grine and Kitching 1987; Wink et al. 1990; Deeming and Ferguson 1991; Wink and Elsey 1994).

Despite the microstructural differences highlighted above, both *MT II/a* and *II/b* share the most characteristic features of crocodilian eggshells (see Marzola et al. 2015 for a review).

Morphotype III (MT III)

MT III makes up only 1% of the total weight of the eggshell fragment assemblage. It is ~250–310 μm thick, and has a featureless, smooth outer surface (Fig. 3L) and a rough inner surface due to the very robust mammillary cones (Fig. 3K). Under SEM and PLM, its three-layered microstructure is well pronounced with barrel-shaped mammillae which locally form variably sized aggregates (~40–160 μm width) in the ML, the narrow (~25 μm) and straight prisms in the PL, and a thin EL (~30 μm) which is separated from the underlying prismatic layer by a distinct line (Figs 10 and 11). The thickness ratio of the three layers is ML:PL:EL = 1:3:0.5. The mammillae show radiating crystal wedges (Fig. 10E, H). These spherulites have a well-defined boundary, with the prismatic layer that defines ML thickness as ~60 μm (Figs 10G and 11D, E). On SEM images, several small holes (Ø: ~2–5 μm) are visible, piercing the mammillary cones (Fig. 10C); these may represent bioerosion traces or, alternatively, original vesicles of gas inclusions close to the membrana testacea or shell membrane (Grine and Kitching 1987). The tips of the cones in some specimens are cratered (Figs 10J and 11C), most probably due to embryonic resorption in the late developmental stage (Kundrát et al. 2008; Agnolin et al. 2012). The horizontal accretion lines in the PL are very densely spaced, fine lines (Fig. 11) that are much more pronounced than either in *MT I* or *MT II*. Regionally, accretion lines appear as lines of discontinuity in the prisms under SEM (Fig. 10E). The EL reveals vertically oriented, ~8- to 10-μm-thick crystal blocks which show up almost transparent in some of the thin sections (Fig. 11C, E). The eggshell has a very low density of pores

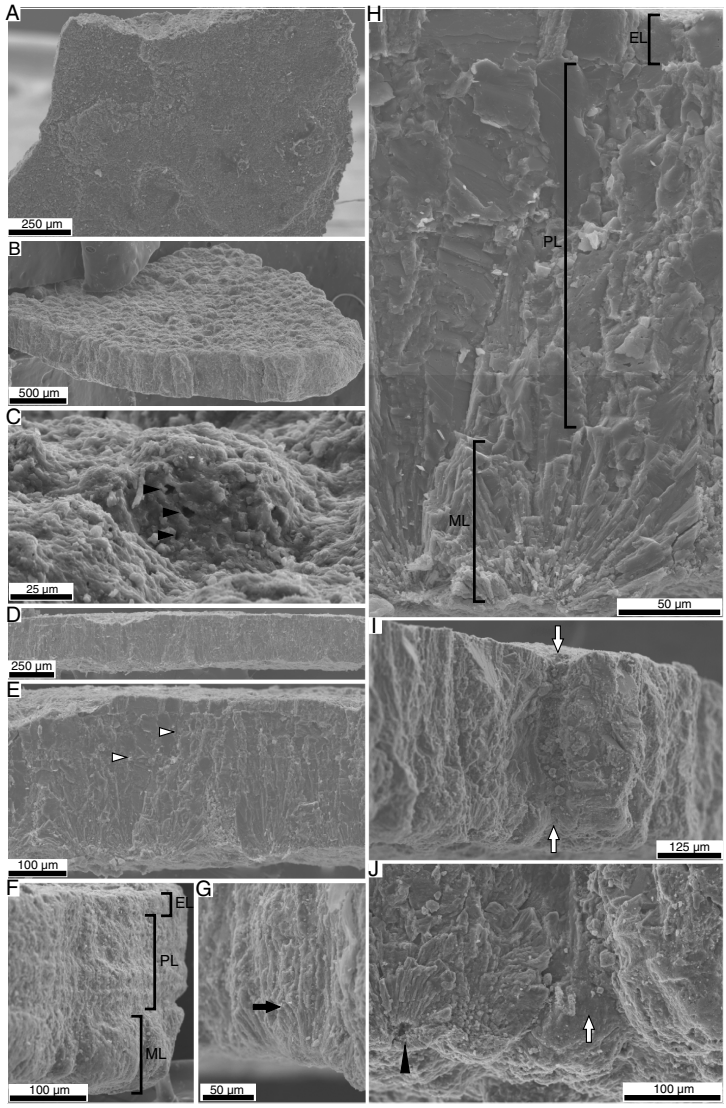

Fig. 10
SEM images of *MT III* specimens. Inner surface in (A), straight and (B), (C), oblique views demonstrating robust mammillary cones and the prismatic structure on the broken radial surface (B). Tiny holes piercing the mammillary cones [black arrowheads in (C)] may represent bioerosion or gas-including vesicles. (D–H) Trilaminate microstructure composed of mammillary layer (ML), prismatic palisade layer (PL), and a thin external layer (EL) is evident in radial view on freshly broken surfaces (D, E, H) as well as on original eroded edges (F). Mammillae are formed of radiating crystals (H) and show a distinct border with the thin prisms of the PL [black arrow in (G)]. Growth discontinuities in the PL can be observed [white arrowheads in (E)]. (I, J) Straight vertical pores (white arrows) run between the prismatic eggshell units having a wider open funnel shape on the inner than on the external side. A small depression at the base of the radiating crystals of the mammilla [black arrowhead in (J)] marks the position of the original organic core

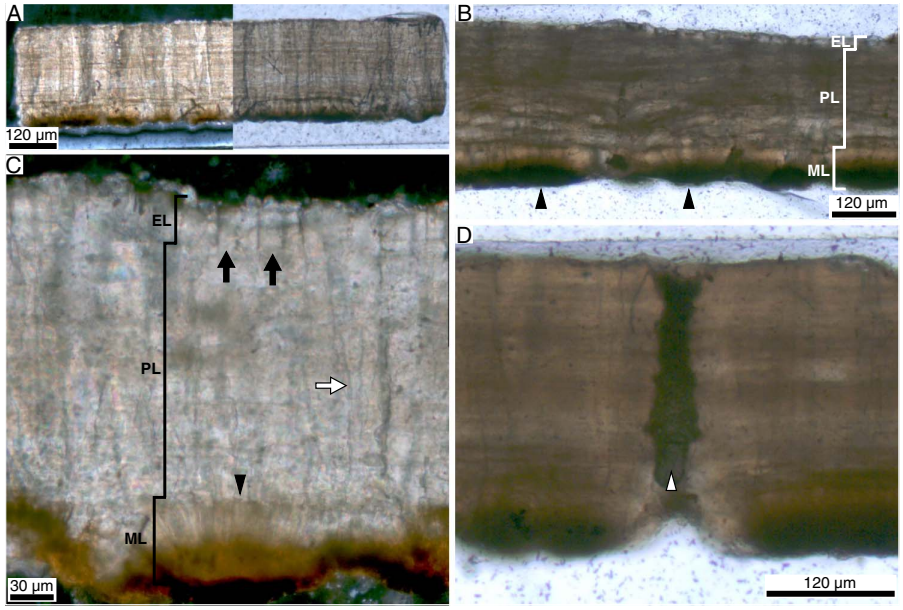

Fig. 11
Thin sections of multiple *MT III* specimens showing different degrees of preservation. Whereas eroded specimens usually exhibit cratered mammillary apices and lack the external layer (A), well-preserved specimens (B, C) present a trilaminate microstructure with robust, locally aggregated barrel-shaped mammillae [black arrowheads in (B)] formed by blade-like spherulite crystals [black arrowhead in (C)] in the mammillary layer (ML), and a distinct external layer (EL) composed of vertical prisms [black arrows in (C)]. The thin prisms [white arrow in (C)] of the palisade layer (PL) are partially obscured by the very dense fine lamination known as tabular ultrastructure. Pores are simple, straight, and columnar [white arrowhead in (D)]

(~0.7/mm^2) and a somewhat higher density of blindly ending pneumatic cavities or incomplete canals (Riley et al. 2014; ~3.8/mm^2) as revealed by µCT investigation (Figs 6C and 7C). The individual pores run between the eggshell units; they are simple, straight, and column-like (Fig. 11F) or funnel-shaped, flaring more on the inner surface (Figs 6C and 10I, J), with an average mid-section diameter of ~27 µm that is ~10% of the mean eggshell thickness. The incomplete canals have similar morphological parameters but do not reach the outer surface (Fig. 6C). Hence, the overall porosity in terms of density of air spaces in the eggshell is the lowest in *MT III* among the three most abundant morphotypes. The structural features of *MT III* are to some extent similar to those of *MT I* and indicate its dinosaurian origin.

Rare morphotypes

Three further morphotypes were recognized in the assemblage, represented by only a single or a few eggshell fragments. Two of these had distinct morphological features

and hence were deliberately selected for investigation. The discovery of the third type, on the other hand, was rather unexpected and happened during thin sectioning of some featureless fragments, of which all but one proved to be eroded *MT III*. The single exception showed pronounced microstructural differences that made its distinction from *MT III* unambiguous.

Among these rare morphotypes, the most abundant one is represented by only five fragments. It shows closely packed angular, mostly triangular knobs of irregular arrangement on the outer surface (Fig. 12A, B), and a coarse inner surface showing mammillary cones (Fig. 12C, D). The diameter of the outer knobs varies greatly between ~20 and 140 μm. The overall eggshell thickness averages around 90–130 μm, including the sculptured areas and the shallow interstices separating the outer knobs. Its microstructure is most similar to that of *MT II*, in particular *II/b*, in having wedge-shaped eggshell units of relatively wide-angled wedges (Fig. 13). As in *MT II*, the mammillary knobs also show large wedges rather than acicular crystal organization (Fig. 13B, C, E, F, H). A single funnel-shaped pore canal was identified in one of the thin sections (Fig. 13B). Even though the distinct ornamentation and the overall thinness clearly distinguish this rare morphotype from both *MT II/a* and *II/b*, based on its general microstructure it is defined here as *MT II/c*; the third subcategory of *MT II*. Accordingly, *MT II/a*, *b*, and *c* are all interpreted as representing eggshells of three different crocodilians. Furthermore, a thin, glass-like transparent fragment demonstrating a rare preservation type was also proven to belong to *MT II/c* when its thin section was investigated (Fig. 14).

The second rare morphotype with distinctive morphological characters, hereafter referred to as *MT IV*, is represented by a single specimen that can be described as having a partially smooth outer surface interrupted by large, bulbous protuberances (Fig. 15A, B). The inner eggshell surface is largely obscured by sediment, but the exposed surface shows coarse irregularities (Fig. 15D). The eggshell is extremely thin; ~30–45 μm in the non-ornamented region and ~60–120 μm in the bulbous areas (Figs 15D and 16). Microstructural preservation of this single specimen is rather poor; however, some features can readily be distinguished. Most importantly, it shows faint but discrete columnar eggshell units which are ~7–9 μm thick, have irregular, rugged outlines, and apparently lack mammillae (Fig. 16C). Only a single, slightly barrel-shaped pore of ~20 μm diameter can be observed with high certainty in the thin section, and it extends through one of the protuberances (Fig. 16C). Nonetheless, the section plane has cut through two other, less well-preserved protuberances that appear to have sediment-filled wider spaces in the same relative position as the pore in the better-preserved protuberance (Fig. 16B, E). On the SEM images, several small holes measuring ~2–3 μm in diameter are present on both the outer and inner surfaces (Fig. 15C); however, these may represent pinholes resulting from acidic erosion by bacterial activity (Smith and Hayward 2010) or abiogenic environmental conditions (Bravo et al. 2003; Clayburn et al. 2004). The general microstructure of *MT IV* could best be described as "geckoid" (Packard and Hirsch 1989; Mikhailov 1991).

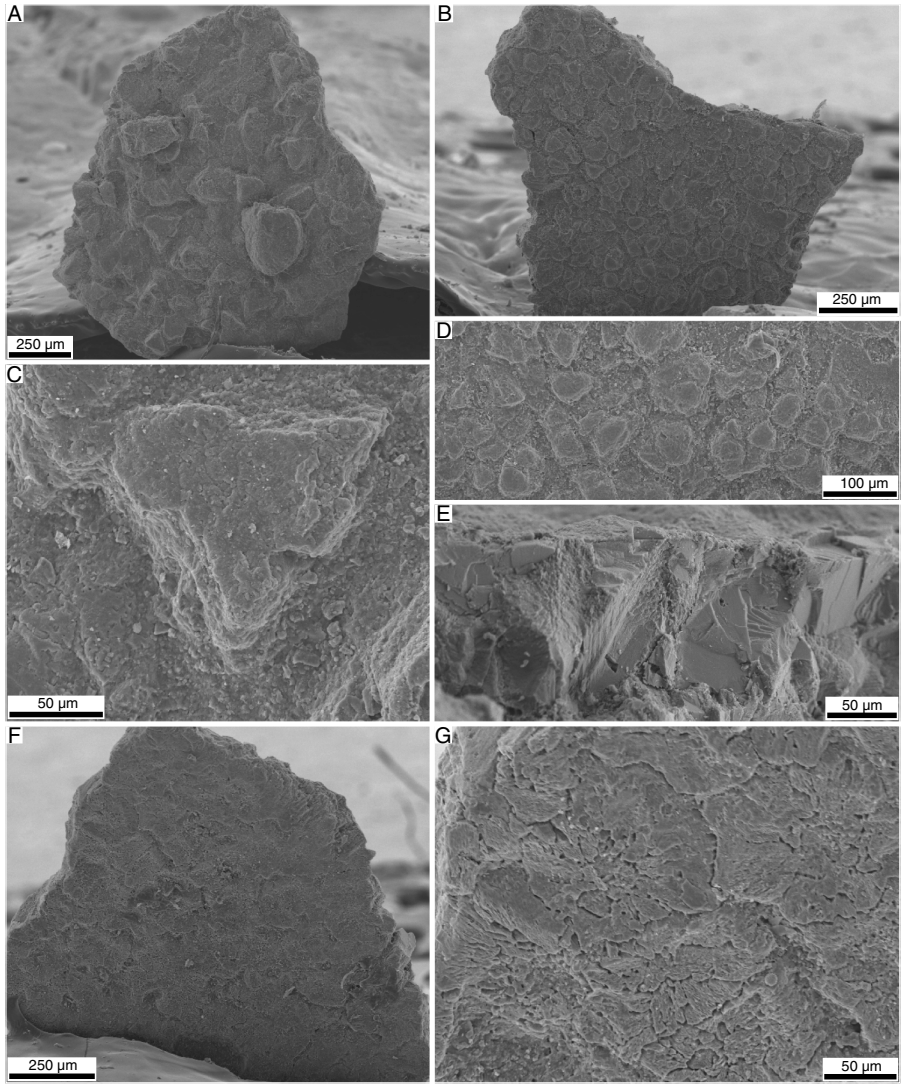

Fig. 12
SEM images of the rare subcategory, *MT II/c*. (A–D) Outer eggshell surface shows triangular ornamental nodes. (E) Broken surface indicates wedge-shaped eggshell units. (F) Inner eggshell surface and (G) close-up of the eroded mammillary knobs of eggshell units

The third rare morphotype, *MT V*, also represented by a single specimen but lacking distinct outer morphology, has revealed a peculiar three-layered microstructure that can be referred to as "ratite" type (Fig. 17). The total eggshell thickness is ~280 µm

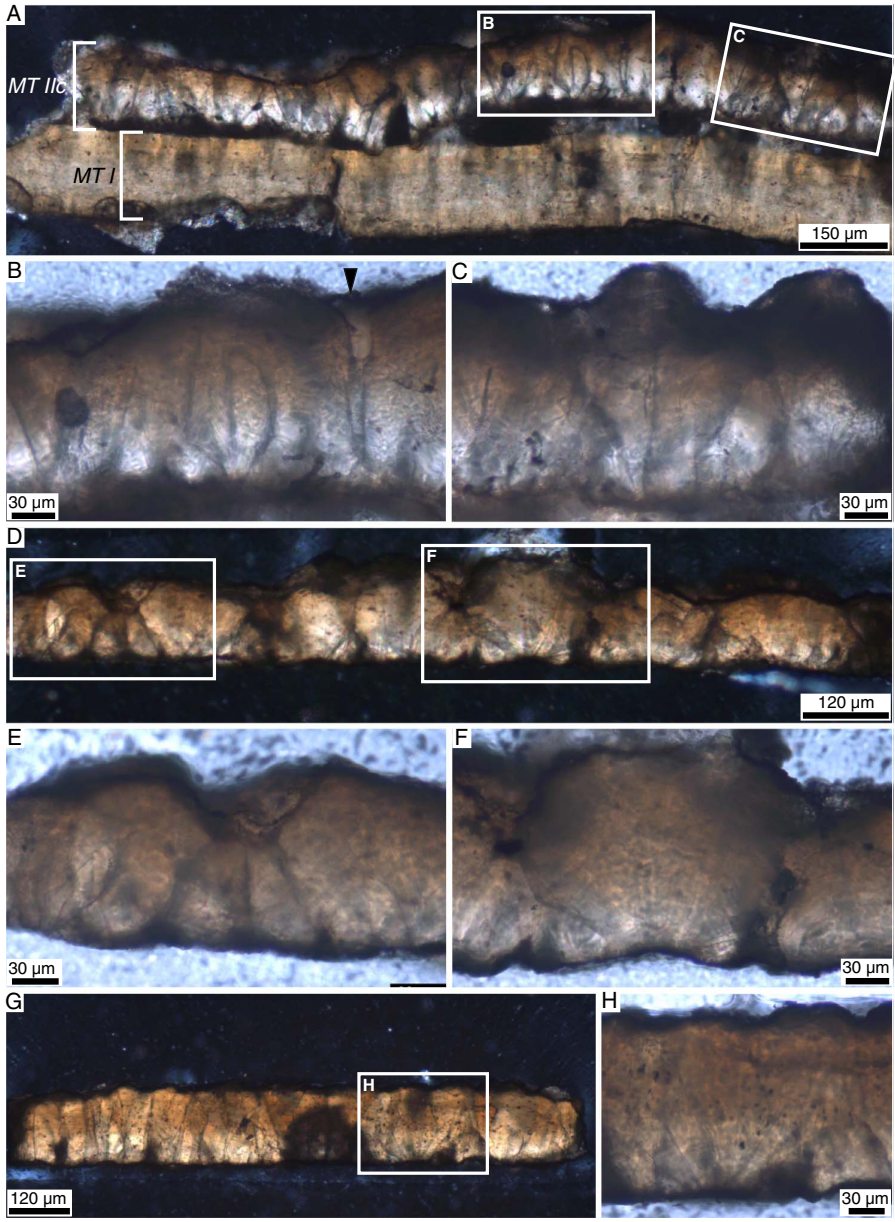

Fig. 13
Thin sections of *MT II/c*. (A–C), (D–F), and (G, H) demonstrate three different fragments, respectively. (A) A rare situation with two different eggshell morphotypes, *MT I* and *MT II/c*, preserved on top of each other being clumped together. Note the overall eggshell thinness in (A), (D), and (G), the wide-angled wedge-shaped eggshell units in (B), (C), (E), (F), and (H), and the funnel-shaped pore canal in (B) (black arrowhead)

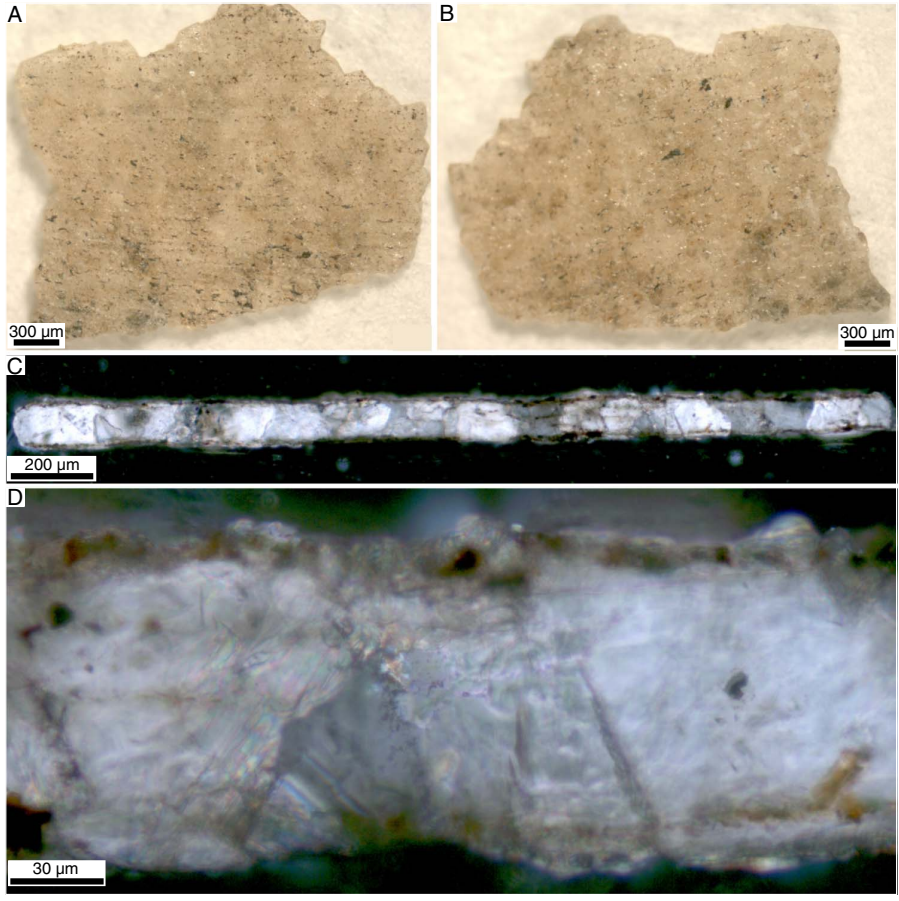

Fig. 14
Rare transparent, glass-like preservation type of *MT II/c*. (A, B) Outer and inner eggshell surface cannot be distinguished under stereo microscope in this transparent specimen. (C, D) Thin section, however, reveals the characteristic wedge-shaped eggshell units

(Fig. 17A), of which the ML is ~80–100 µm thick, being abruptly separated from the continuous layer (CL) by a well-defined line (Fig. 17B). The apex of the individual mammillae is hardly distinguishable due to strong diagenetic staining and possibly embryonic erosion. The well-preserved part of the mammillae does not reveal any radial crystals but is composed of extremely slender (~3–5 µm) and densely packed prism-like structures with unusually long parallel-running vertical edges (Fig. 17B). The expected but not observed radial spherulites were most probably restricted to the diagenetically affected or eroded apical part of the mammillae. The lack of definite

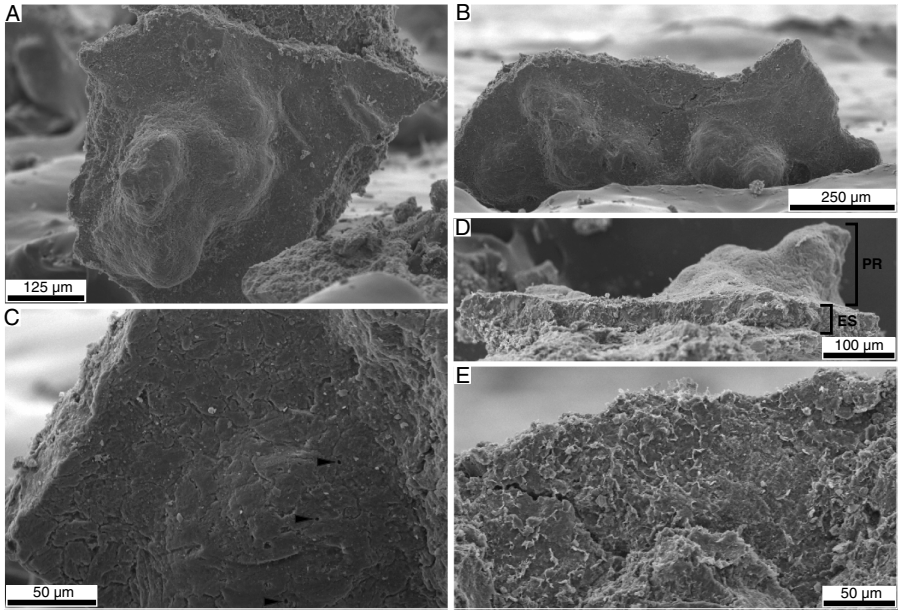

Fig. 15
SEM images of *MT IV*. (A, B) Bulbous protuberances characterize the ornament morphology. (C) Close-up of the network of micro-fissures on the outer shell surface showing pinholes (black arrowheads). (D) Radial view on the fragment revealing the extreme thinness of the shell (ES) and the robust protuberance (PR). (E) Indistinct, rough inner eggshell surface

mammillary apical regions and the preserved, closely spaced, parallel-running vertical prisms forming each mammilla make the distinction of individual mammillae impossible. However, more pronounced interstices occasionally present among the slender prisms of the ML may indicate the borders of individual mammillae (Fig. 17B). The overall ultrastructure of the CL is squamatic, although further stratification within this layer can also be observed (Fig. 17A). The two sublayers in the CL are equal in thickness (~80 µm) and separated by a distinct line. The characteristic "herringbone" pattern is more pronounced in the upper sublayer than in the lower one. An additional horizontal discontinuity line runs approximately in the middle of the lower sublayer, but the two halves do not seem to differ in their ultrastructure. The EL is ~25 µm thick, but its ultrastructure is largely obscured by diagenetic staining. In a restricted area, however, faint vertical lines appear in this layer, forming ~1.5 µm thin prisms (Fig. 17B). The thickness ratio in this trilaminate microstructure is ML:CL:EL = 1:2:0.25. No pore was present along the 1.3 mm length of the single thin-sectioned fragment. The listed structural features of this eggshell fragment suggest a dinosaurian egg layer.

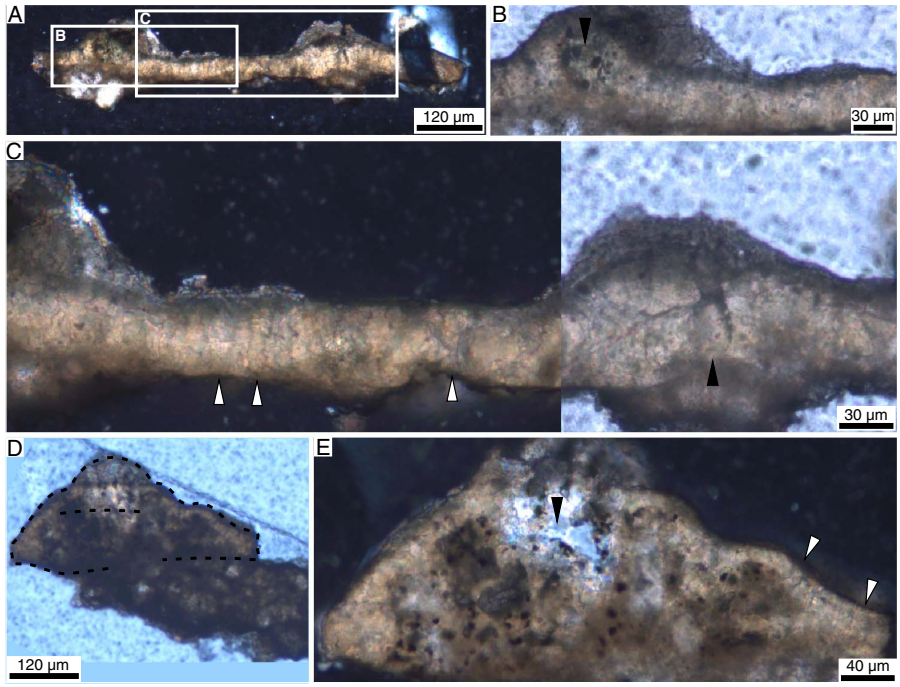

Fig. 16
Thin section of *MT IV* revealing microstructural features not able to be observed in SEM. Both the bigger (A–C) and smaller (D, E) fragments of *MT IV* are characterized by columnar eggshell units lacking mammillae [white arrowheads in (C) and (E)], a simple, slightly bulking pore canal [black arrowhead in (C)] and other two putative pore canals filled with sediment crystals [black arrowhead in (B) and (E)] that perforate the eggshell in the bulbous areas. The smaller fragment in (D) (outlined with black dashed line) shows a thick layer of sediment attaching to its base

Quantitative uni- and bivariate analyses

Multiple measurements taken of each variable along the length of five thin sections of each major category, *MT I*, *MT II* (*a*, *b* together), and *MT III* revealed that the different microstructural characters show a wide range of variation (Table 2) and in some cases non-normal distribution even within a single fragment. For instance, right-skewed distribution of mammilla width measured at the level of contact between two adjacent mammillae (Fig. 2) seems to be the normal condition in the specimens of all three morphotypes. Even though the other variables commonly show normal distribution within a single specimen, when specimen data are pooled in each morphotype, most of the variables acquire a non-normal distribution. Since it was impossible to determine which eggshell fragments could have belonged to the same egg, the

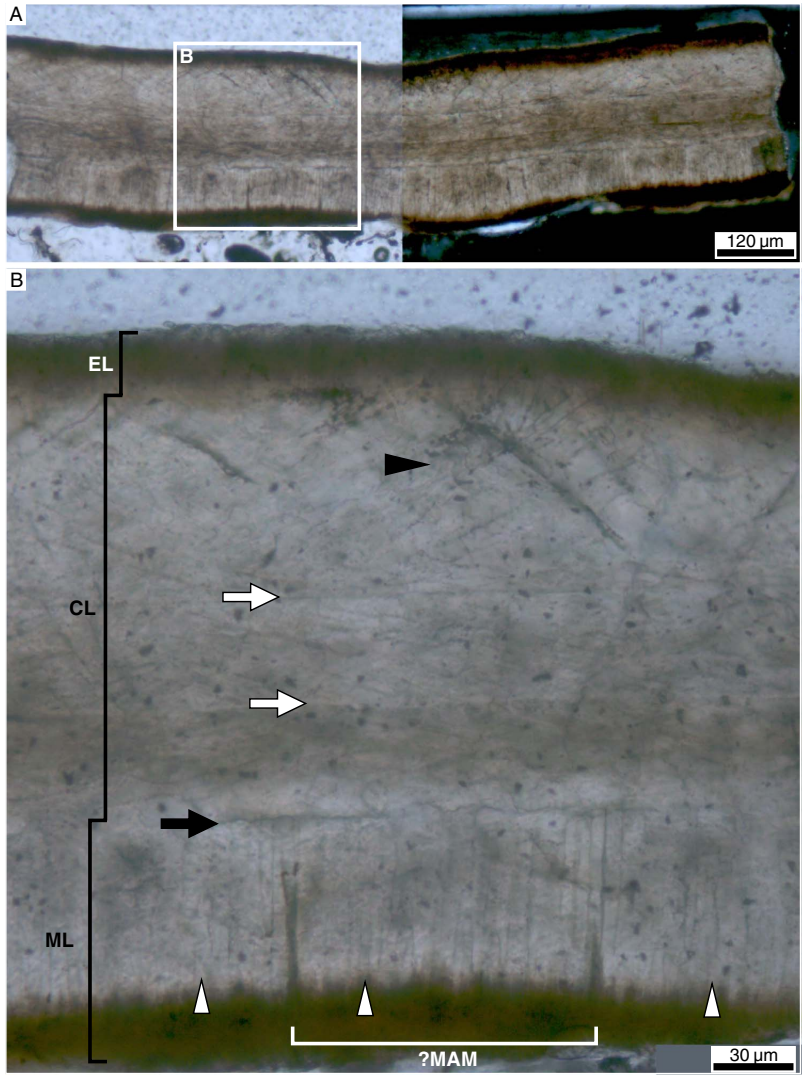

Fig. 17
Thin section of the single specimen of *MT V*. (A) Full extent of the fragment and (B) a magnified area demonstrating a trilaminate microstructure with a thick mammillary layer (ML) composed of extremely slender, long, and parallel-running vertical prisms [white arrowheads in (B)], a squamatic continuous layer (CL) subdivided into further layers by fine horizontal lines [white arrows in (B)], and a thin external layer (EL) showing faint vertical crystal blocks. Individual mammillae are difficult to distinguish due to erosion and diagenetic coloration of the mammillary apices; however, more pronounced interstices among slender prisms may indicate the borders of individual mammillae (?MAM). The mammillary and continuous layers are separated by a distinct line [black arrow in (B)], whereas diagenetic staining obscures the border between the continuous and external layers. The upper third of the continuous layer reveals the well-known "herringbone" pattern [black arrowhead in (B)]

non-normal distribution of variables in the pooled data set demonstrates great intra- and/or inter-individual variability in these characters.

Despite the considerable microstructural similarities between eroded fragments of *MT I* and *MT III* with indistinct ornamentation and weathered mammillary cones, non-parametric permutation tests revealed those reliable characters which can be used to distinguish these two morphotypes even in poorly preserved specimens. The total eggshell thickness, ML thickness, mammilla width, PL thickness, and prism width of *MT I* are significantly less than those of *MT III*, whereas the EL thickness is equal in the two morphotypes (Table 3).

As for *MT II*, the three subcategories can also be distinguished based on five, three, and four specimens of *II/a*, *II/b*, and *II/c*, respectively (Table 4). The angle of the wedge-shaped shell units is smaller in *II/a* than in either *II/b* or *II/c*, but it is equal in the latter two. ML thickness in *II/a* and *II/b* is equal and both significantly exceed that in *II/c*. Width of mammillae is greatest in *II/b*, followed by *II/a* and finally *II/c*. Second ("palisade") layer thickness is largest in *II/a*, followed by *II/b*, and *II/c* has the thinnest second layer (Table 5).

Multivariate analyses

Different multivariate methods, which complemented the bivariate analyses in checking the reliability of our qualitative morphotype categorization, gave largely consistent results, albeit some particulars differed in some cases. In line with the qualitative results, a data set was created for the multivariate separation of *MT I*, *MT II*, and *MT III* (five specimens each), and another one to explore the validity of the subdivision of *MT II* into *II/a*, *II/b*, and *II/c* (five, four, and three specimens, for the respective subcategories). As only continuous numeric characters were used in these

Table 3
Relationship of morphometric variables between the two microstructurally similar morphotypes, *MT I* and *MT III*. Only external layer thickness is equal in *MT I* and *MT III*, whereas all other variables have lower values in *MT I* than in *MT III*

Variable	Relationship	*p*-Value (non-parametric permutation test)
Th	*MT I* < *MT III*	$p < 0.0001$
MW	*MT I* < *MT III*	$p < 0.0001$
MTh	*MT I* < *MT III*	$p < 0.0001$
PTh	*MT I* < *MT III*	$p < 0.0001$
PW	*MT I* < *MT III*	$p < 0.0001$
ETh	*MT I* = *MT III*	$p = 0.2881$

Table 4
Mean and corresponding standard deviation (SD) values of different morphometric variables calculated from data of *MT II*: *II/a*, *II/b*, and *II/c*

MT II subcategory	SUA	MW	MTh	PTh
II/a mean	28.49	65.82	42.70	193.35
II/a SD	8.99	20.71	13.09	55.07
II/b mean	63.10	105.18	51.35	147.00
II/b SD	9.59	18.64	10.74	21.67
II/c mean	65.49	54.92	24.15	93.60
II/c SD	19.78	15.67	3.86	22.51

Table 5
Relationship of morphometric variables among the three subcategories of *MT II*: *II/a*, *II/b*, and *II/c*. The demonstrated highly significant differences allow secure quantitative differentiation of the three structurally very similar *MT II* subcategories

Variable	Relationship	*p*-Value (non-parametric permutation test)
SUA	$II/a < II/b = II/c$	$p < 0.0001$; $p = 0.4966$
MW	$II/c < II/a < II/b$	$p = 0.0154$; $p < 0.0001$
MTh	$II/c < II/a = II/b$	$p < 0.0001$; $p = 0.1832$
PTh	$II/c < II/b < II/a$	$p < 0.0001$; $p = 0.0005$

analyses, surface ornamentation features were not included as variables, the lack of which considerably decreases the power of separation of the different morphotypes and subcategories.

Analyses of MT I, MT II, and MT III

The PCA performed on standardized data of specimens selected from the three morphotypes revealed two important principal components (PC) explaining 72.31% and 24.22% of the total variance, respectively. Positive correlation between mammilla width and the other variables, as well as between thickness of ML and PL accounts for the large contribution of PC1 to the total variance with all four variables having approximately equal and positive loadings. Specimens of *MT I* are closely associated and plot separately from the other specimens; however, *MT II* and *MT III* specimens do not form two distinct groups along PC1 (Fig. 18A).

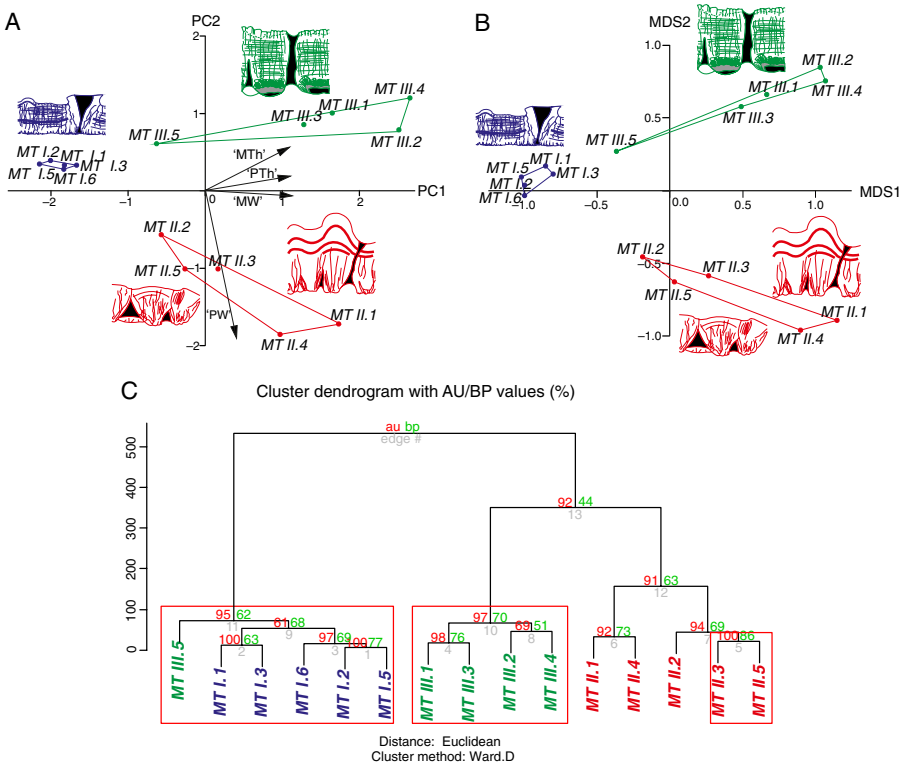

Fig. 18
Graphical output of multivariate morphometric analyses of *MT I*, *MT II*, and *MT III*. *MT I*, *MT II/a, b*, and *MT III* specimens are marked with blue, red, and green, respectively. Schematic color-coded line drawings of the morphotypes in (A) and (B) are placed adjacent to their groups visualized by PCA and NMDS. (A) PCA reveals *MT I* as the most coherent group, as it shows no overlap with the other two groups on either PC-axis. Arrangement of specimens and variable loadings (black vectors) show that PC1 and PC2 reflect absolute size and eggshell unit morphology, respectively. For codes of variables, see Table 1. (B) NMDS in principle shows the same intra- and intergroup specimen distributions as PCA. (C) Cluster analysis recovers three significant clusters (AU > 95%) indicated by red squares consisting of: 1, all *MT I* and a single *MT III*; 2, the rest of *MT III* specimens; 3, two *MT II* specimens

Knowing that *MT I* is the thinnest eggshell morphotype, whereas *MT II* and *MT III* have similar thicknesses, PC1 is interpreted as representing an absolute size measure. On the other hand, members of the three morphotypes are separated along PC2 without overlap (Fig. 18A). Here, prism/eggshell unit width is the dominant factor and is negatively correlated with PC2. The position and distinct separation of specimens of *MT II* from *MT I* and *MT III* specimens along PC2 clearly demonstrates that PC2 reflects differences in overall morphology of the eggshell unit, with *MT I* and *MT III* possessing a prismatic PL, and *MT II* showing wedge shaped units. PC1-2 scatterplot

shows that the morphologically most homogeneous and heterogeneous groups are formed by *MT I* and *MT II*, respectively (Fig. 18A). NMDS ordination with a stress level of 0.02596 gave results broadly similar to PCA: only *MT I* grouped separately on axis1, whereas on axis2 specimens of each morphotype were distributed in their respective groups without overlap with members of the others (Fig. 18B). However, as with PC2, *MT I* and *MT III* once again plot closer together than either of them to *MT II* on NMDS axis2, suggesting the importance of eggshell unit morphology in ordination of the specimens.

Interestingly, agglomerative hierarchical cluster analysis (Fig. 18C) grouped members of *MT II* and *MT III* closer to each other except for one *MT III* specimen which was grouped in the same significant cluster (AU% = 95) as all *MT I* specimens. This single *MT III* specimen is unusually thin for its morphotype probably due to embryonic and/or surface erosion which may explain its clustering together with the microstructurally similar thinnest morphotype *MT I*. Nevertheless, the rest of the *MT III* specimens also formed a significant group (AU = 97%), whereas neither the *MT II–MT III* cluster, nor the cluster composed only of *MT II* specimens, was significant. Only two *MT II* specimens were grouped together in a highly significant cluster (AU = 100%).

Analyses of MT II/a, b, c

PCA identified two important PCs contributing to the total variance of standardized data of *MT II* specimens by 63.25% and 32.54%, respectively. Only *MT II/c* specimens grouped separately along PC1, whereas specimens of *MT II/a* and *II/b* plotted in the same range with *II/a* specimens spreading over the largest PC1 interval (Fig. 19A). Variables on PC1 had approximately equal contributions and only eggshell unit angle correlates positively with PC1. The position of the specimens and the variable loadings suggest that PC1 corresponds to an absolute size measure with its negative range representing larger sizes. PC2 separates *MT II/b* from both *II/a* and *II/c*, whereas the position of some specimens of the latter two subcategories overlap. Here, the angle of the wedge-shaped eggshell unit and mammilla width are the most important variables. All variables except for PL thickness correlate negatively with PC2, implying that PC2 corresponds to eggshell unit morphology describing forms of broader or narrower wedges. In this respect, *II/c* seems to have the largest variability (Fig. 19A).

Ordination by NMDS with a stress level of 0.00498 showed essentially the same arrangement of specimens (Fig. 19B) as the PCA plot, therefore, the interpretation of the axes of the two-dimensional ordination is also similar to PC1 and PC2.

Cluster analysis (Fig. 19C) revealed an overall closer relationship between *MT II/b* and *II/c*; however, a single specimen of *II/a* was attached to the cluster of *II/c*, whereas the rest of *II/a* specimens formed a separate and significant cluster (AU = 97%). All *II/b* specimens were grouped into a significant cluster (AU = 97%), whereas *II/c* specimens were divided into two significant clusters (AU = 99% and 96%). The overall pattern of clustering, including the separation of a single *II/a* specimen from

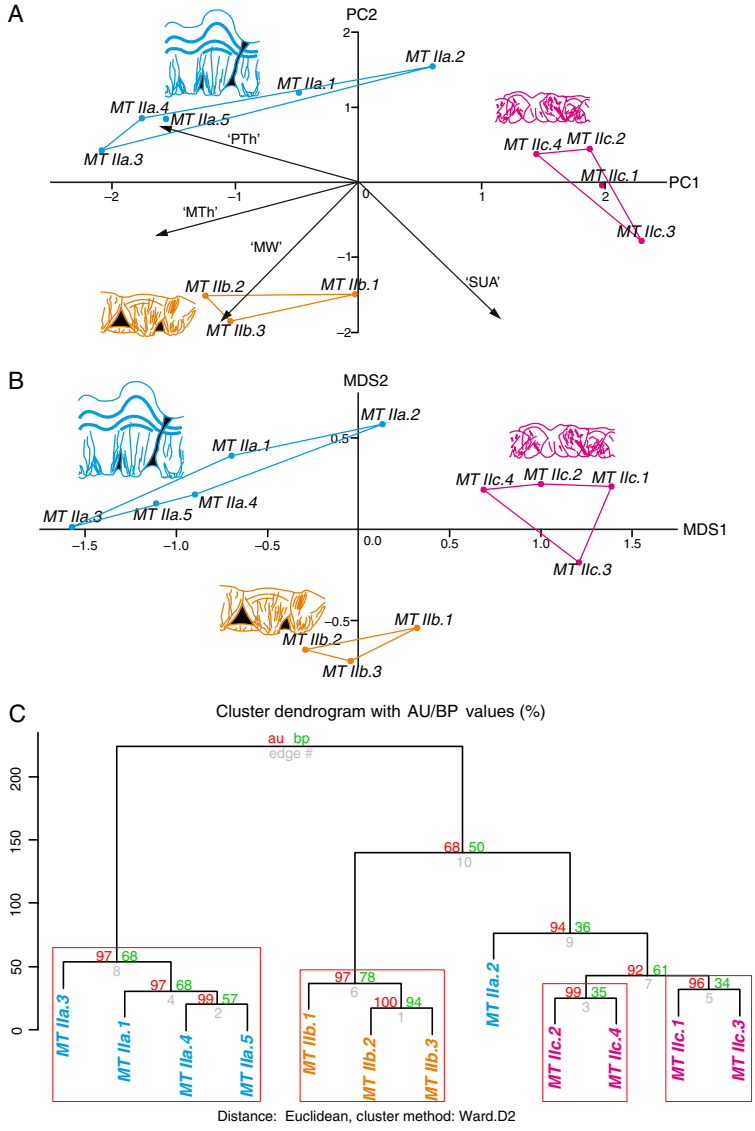

Fig. 19
Graphical output of multivariate morphometric analyses of the three *MT II* subcategories. *MT II/a*, *II/b*, and *II/c* are marked with light blue, orange, and purple, respectively. Schematic color-coded line drawings of the *MT II* subcategories in (A) and (B) are placed adjacent to their groups visualized by PCA and NMDS. (A) PCA demonstrates *II/c* and *II/b* as being the most distinct groups on PC1 and PC2, respectively. Specimen arrangement and variable loadings (black vectors) identify PC1 as absolute size, and PC2 as eggshell unit shape. For codes of variables, see Table 1. (B) NMDS shows the same intra- and intergroup specimen distributions as PCA. (C) Cluster analysis recovers four significant clusters (AU > 95%) indicated by red squares showing consistent grouping of *II/b* and all but one of *II/a* specimens, but dividing *II/c* into two groups

the rest of its subcategory, is in line with the multivariate visualization plots of PCA and NMDS and suggests the same underlying factors dominating the topological arrangement of specimens belonging to different *MT II* subcategories.

μXRF

μXRF scan results gained from the combination of qualitative color maps, line scan, and semi-quantitative net photon count data provided valuable information on the composition and concentration patterns of different elements in the eggshell fragments. Clearly, calcium is the most dominant element in all specimens followed by P, S, K, and Ni. The latter, somewhat unexpectedly, also occurs at relatively high concentration in every fragment (Figs 20 and 21A, B, D). Fe is usually present within the eggshells, but gives the strongest signal close to the surfaces, appearing as a crust over the specimens. Other elements, such as Mg, Al, Ba, Mn, and some trace and rare earth elements (REE; e.g., Ti, Sr, Ce) also occur (Figs 20 and 21B–H) in the fragments. Cl is evidently predominant in the glue and/or epoxy resin used to stabilize and embed the specimens, but other elements, for example, Si, Mg, Zn, Cu, and Ga, are also prevalent as compared with the eggshells. In contrast to the eggshells, Ca, P, and S are of very low concentration or absent in the resin and glue, and REE seem to be largely absent or present only in very low amounts in the embedding media. Thus, element composition of the eggshell fragments can readily be distinguished from that of the resin and glue which allowed us to account for the distorting effect of the embedding medium while evaluating the chemical composition of eggshells.

Surface scans of a few ornamented shell fragments illustrate the effect of pore spaces trapping sediment matrix (Fig. 20A), where elements such as Fe and S were both abundant in the pores, possibly in the form of pyrite. Interestingly, in other specimens, S and Fe did not show any spatially coinciding peaks (Fig. 20D) that would indicate the presence of pyrite. Thus, in sharp contrast with most of the fossils known from the Iharkút locality (Botfalvai et al. 2015, 2016), pyrite seems to have played no role in the preservation of these fragile eggshell fragments.

Some specimens show distinct compositional features in terms of frequently revealing the highest or lowest concentrations of certain elements. Spectral peaks show that one of the *MT I* specimens and the single *MT II/c* with glassy, transparent appearance record by far the highest and the second highest abundance of Si, as compared with the other specimens (Fig. 21E). Furthermore, the same *MT I* specimen shows the highest concentrations of Mg, Al, Cl, Fe, Ti, and V, but the lowest Ca (Fig. 21). The *MT II/c* fragment has the highest concentrations of Ni, Cu, and Zn. However, individual color maps of element distributions and line scans of element concentrations on the radial sections of these fragments reveal that Si and Cl actually drop within the eggshells as compared with the surrounding resin and glue. Apart from Ca, P, S, and K peaks present in all specimens, the only other elements which consistently peak within these *MT I* and *MT II/c* fragments are Fe, V, and Ti in *MT I* and Ni in *MT II/c*. In addition, one *MT III* fragment also deviates from the average

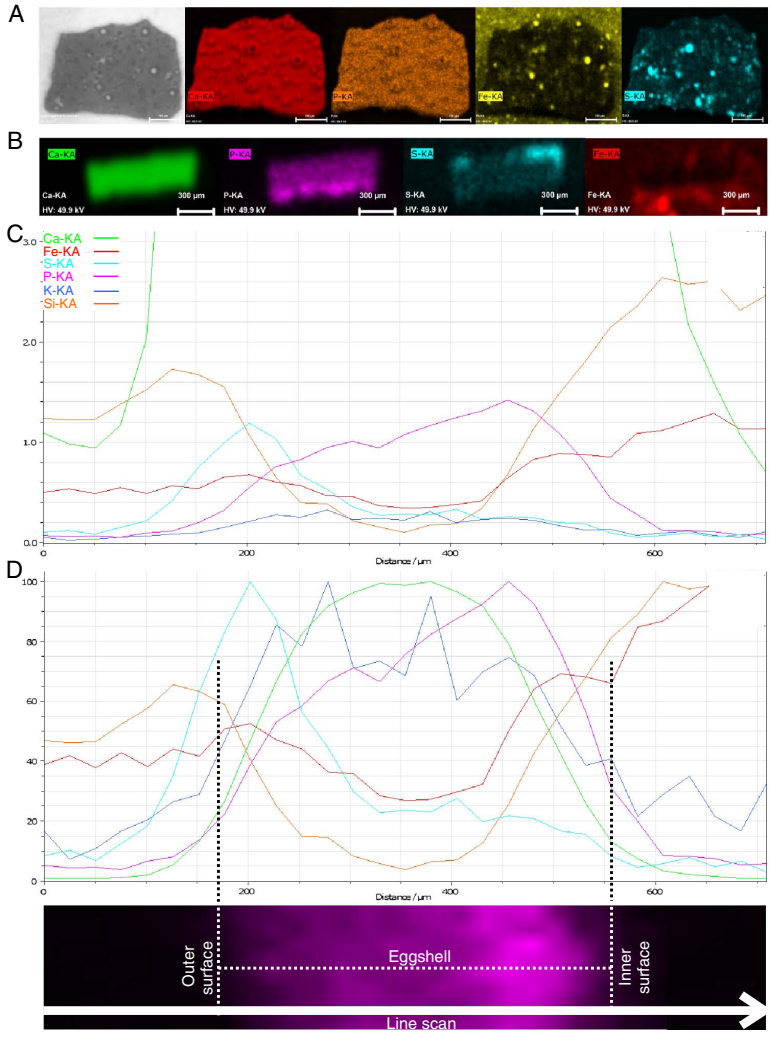

Fig. 20
Element composition maps and line scan of µXRF analysis. (A) Color maps of the external surface of an *MT I* specimen not embedded in resin. Note the strong Fe signal in the sediment stuck in the crater-like surface ornamentation. Only partial correspondence between visual signals of Fe and S can be observed which may indicate pyrite. (B) Color maps visualizing Ca (green), P (magenta), S (blue), and Fe (red) content in a radially cut *MT III* specimen embedded in resin. Note the higher concentration of P in the mammillary cones. (C, D) Line scan results of specimen in (B) along dashed line shown in (D). (C) Relative abundances of the major elemental components expressed as percentages of the most abundant element (Ca set as 100%). (D) Concentration of major elements relative to their own maximum along the transect line. Ca, P, and K show highest abundance peaks within the eggshell, whereas S and Fe abundance increases at the eggshell surface. Si is mostly outside of the eggshell's range. Ca is clearly overwhelming (see also B, C), followed by P which shows a slight increase toward the inner eggshell surface, in line with the higher P content in the mammillary cones revealed by element color mapping (B)

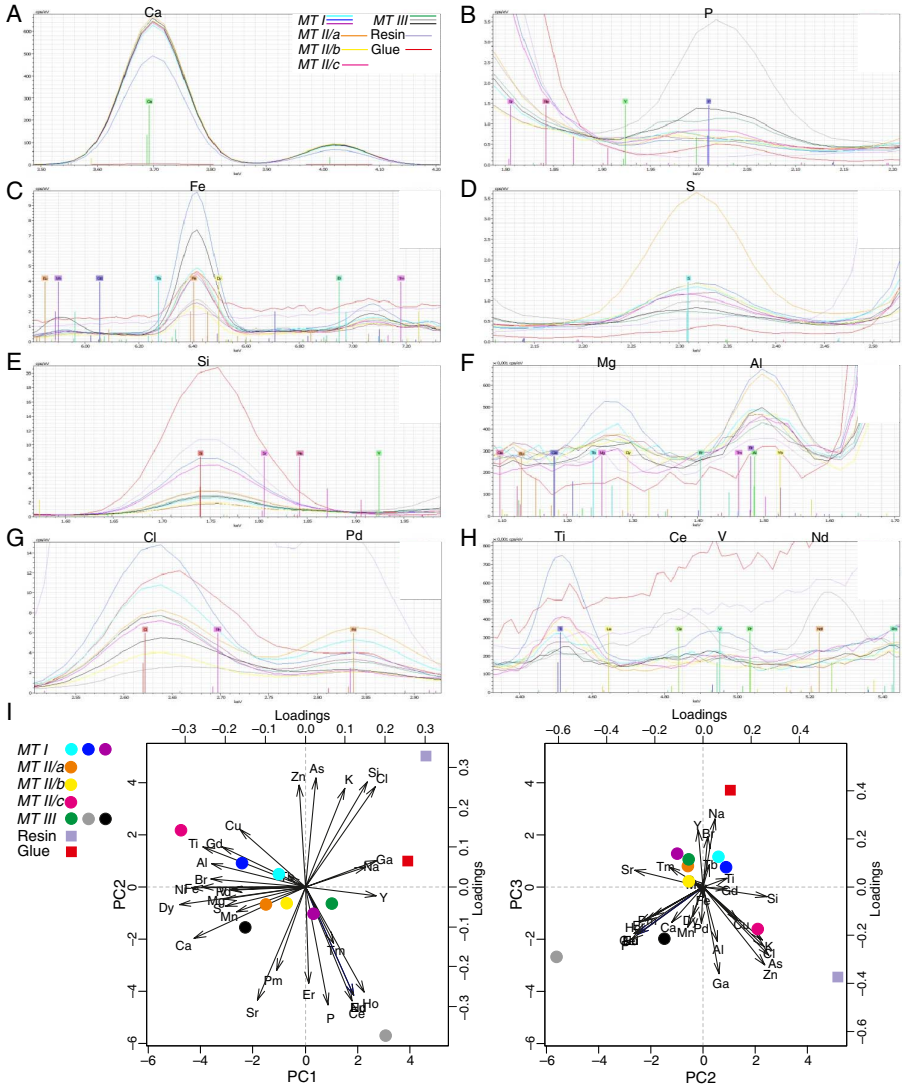

Fig. 21
Element analysis with μXRF spectroscopy. (A–H) Spectral output for major elements Ca (A), P (B), Fe (C), S (D), Si (E), Mg and Al (F), Cl and Pd (G), and Ti, Ce, V, and Nd (H). Note the near absence of Ca but overwhelming majority of Cl and Si in both the epoxy resin (bluish gray) and glue (red). Ca peak is also significantly lower in one of the *MT I* specimens (dark blue), whereas the same specimen shows the highest peaks in Fe, Si, Mg, Al, and Cl among the eggshell specimens. An *MT III* specimen (gray) shows the highest P, but also Ce and Nd. (I) Visual output of PCA demonstrates that general chemical composition of the eggshell specimens is similar, with the exception of an *MT III* specimen (gray) appearing separately on both PC1–PC2 and PC2–PC3. *MT II/c* (magenta) displaying special translucent/glassy preservation also plots farther from the rest of the specimens on PC2–PC3 (see main text for discussion)

spectra by showing the highest abundance of P and the only peaks for two REE, Ce and Nd (Fig. 21B, H). The highest density of P can be observed in the ML on the color map (Fig. 20B) that corresponds to the line scan along the transect of the shell showing a peak in P in the internal surface of the eggshell fragment (Fig. 20B, C).

The PCA (Fig. 21I) performed on the spectral data shows that most specimens have largely similar chemical composition with the exception of the *MT III* fragment (gray circle in Fig. 21I). This outlier *MT III* specimen is separated from the rest of the fragments on both PC1–PC2 and PC2–PC3 plots, due to the highest P content and the presence of two REE, Ce and Nd. In addition, the transparent *MT II/c* specimen also appears separately on the PC1–PC2 plot. Percentages of variance explained by the components gradually decreased (26.2% PC1, 21.5% PC2, 13.7% PC3, etc.), and no strong correlation in the abundance relationships of different elements can be observed.

Discussion

Identification of egg layers

MT I. The most abundant eggshell morphotype at Iharkút, *MT I*, shows a ML and a compact prismatic PL (Figs 4 and 5) verifying its dinosaurian origin and the rigid nature of the original eggshell (Packard and Demarco 1991). The intact shell is relatively thin, implying a small egg size: based on the relationship between calcareous eggshell thickness and egg mass in the rigid-shelled eggs of birds (Ar et al. 1979), *MT I* may have weighed about 8–15 g; a mass range corresponding to that of dove eggs (*Streptopelia*). The surface ornamentation of *MT I* is virtually identical with that demonstrated in the "geckoid" eggshell fragments reported from the Maastrichtian Rusca Montană Basin, Romania (Vasile and Csiki 2011; Csiki-Sava et al. 2015). Furthermore, this Romanian eggshell type has almost the same thickness (~170 µm; Vasile and Csiki 2011) as the mean thickness of *MT I* (~160 µm). However, the lack of detailed description and images of microstructural characters prevents any further well-founded comparison. The overall macro- and microstructure of *MT I* is extremely similar to those of the ootaxon *Pseudogeckoolithus* known from the Maastrichtian strata of Spain and France (Vianey-Liaud and López-Martínez 1997; Garcia 2000) as well as several fragments of a yet unnamed eggshell morphotype from Vitrolles-Couperigne and La Neuve, France, that was referred to as "geckonoid" by Garcia (2000). The uniquely shared features uniting *MT I*, *Pseudogeckoolithus*, and the unnamed "geckonoid" are the characteristic surface ornamentation combined with the "dinosauroid-prismatic" microstructure and that most pores open onto the outer shell surface through the tubercles creating smaller holes in the nodes (*Pseudogeckoolithus*, unnamed "geckonoid") or more crater-like rings (*MT I*). This latter condition has also been reported in the Late Campanian ootaxon *Porituberoolithus* with uncertain theropod affinities (Zelenitsky et al. 1996; Tanaka et al. 2011) but not in any other

dinosaurian eggshell type to date. In all three, *MT I*, *Pseudogeckoolithus*, and the unnamed "geckonoid," the pores run vertically or slightly obliquely and have about the same diameter in relation to total eggshell thickness in non-sculptured areas (~12%–15%). They show a thin ML with relatively slender, conical, and densely spaced mammillae and fine lamination in the prismatic PL, features that were also demonstrated in the eggshell of the Late Jurassic allosauroid *Lourinhanosaurus* (Mateus et al. 1997), as well as the Late Cretaceous oospecies *Triprismatoolithus stephensi* attributed to a theropod dinosaur (Jackson and Varricchio 2010), and even in the extant ratite bird *Struthio* (Zelenitsky and Modesto 2003). The overall "dinosauroid-prismatic" microstructure and the demonstrated similarities with the latter taxa clearly speak for a theropod, most probably maniraptoran origin of both, *MT I* and *Pseudogeckoolithus*. Even though the unnamed "geckonoid" eggshells have originally been separated from *Pseudogeckoolithus* eggshells based on their thinness (~220 μm vs. ~300 μm) and higher density of ornament nodes (Garcia 2000), here we consider this eggshell morphotype as belonging to theropod dinosaurs as well. Apart from such slight differences in thickness and outer sculpture, these three eggshell types undoubtedly form a distinct group, with the egg layers most likely having been closely related theropod taxa. Although the "geckoid" eggshell fragments recovered from Romania (Csiki et al. 2008; Grigorescu and Csiki 2008; Vasile and Csiki 2011; Csiki-Sava et al. 2015, 2016) have been tentatively assigned to squamates (Csiki-Sava et al. 2015, 2016), the identical ornamentation and thickness of these fragments and *MT I* strongly suggest the same, closely related theropod affinities for the eggshell fragments from Romanian, Spanish, French, and Hungarian localities. This places *MT I* and the other two unnamed "geckoid/geckonoid" types among the thinnest fossil theropod eggshells reported to date, the thinness of which is only rivaled by the eggshells of the smallest avian eggs known from the Mesozoic record, such as those of enantiornithine birds (Sabath 1991; Fernández et al. 2013; Kurochkin et al. 2013; Zhang et al. 2015). As most extant and fossil avian eggshells have smooth surface and a pronounced trilaminate microstructure (e.g., Mikhailov 1997; Schweitzer et al. 2002), the avian nature of the strongly ornamented *MT I* with questionable presence of an EL is uncertain at best. Embryonic remains would be necessary to elucidate whether *MT I* is among the thinnest fossil avian eggshells or represents the thinnest non-avian theropod eggshell described to date.

Based on inferred egg size, the egg layer of *MT I* was probably a smaller-bodied theropod than that of *Pseudogeckoolithus* but similar-sized as the parent taxon of the eggshells from Romanian and French localities. Although calculation of gas and water conductance is not possible due to the fragmentary nature of all eggshells, the thinness of *MT I* combined with a moderate to high density of pores and blindly ending pneumatic cavities (Table 2), and the wide pores relative to overall shell thickness suggest that the eggs were deposited in a buried nest, as reconstructed for most dinosaurs (Williams et al. 1984; Horner 2000; Deeming 2006), and probably representing the ancestral mode of egg-laying (Tanaka et al. 2015).

MT II. *MT II* is composed of three different subcategories, all sharing crocodilian-like eggshell microstructure (Figs 8, 9, and 12–14). However, as opposed to the findings in multiple crocodylomorph eggshells (Moreno-Azanza et al. 2014; Marzola et al. 2015), a third compact outer layer could not be distinguished and the tabular ultrastructure of the wedge-shaped eggshell units was not evident in SEM images. Instead, horizontal accretion lines in form of growth mark-like bands and finer lines following the undulation of the surface sculpture were clearly observed in thin sections (Fig. 9). As the multilayered tabular nature of fossil crocodilian eggshells is not always evident and may require special preservation, treatment, and/or visualization techniques (Hirsch 1985; Moreno-Azanza et al. 2014), the lack of such observable ultrastructural features in *MT II* eggshells does not exclude their crocodilian affinities.

The detected differences among *II/a*, *II/b*, and *II/c* suggest different egg-laying crocodylomorph taxa. Whereas *MT II/a* and *II/b* show comparable absolute dimensions, *II/b* and *II/c* are more similar in their eggshell unit morphology with wider angle of the wedge-shaped units (i.e., higher width to height ratio). The similar thickness and slight ornamentation differences of *II/a* and *II/b* could suggest that these eggshell subcategories might have belonged to the eggs of the same crocodilian egg layer. In fact, diversity in surface ornamentation along the longitudinal axis of a single egg has been demonstrated in crocodilian eggshells (Marzola et al. 2015). However, differences in eggshell unit morphology observed and quantitatively verified between *II/a* and *II/b* imply that these subcategories were produced by two different taxa. Because *II/c* is considerably thinner than both *II/a* and *II/b* and has a distinct surface sculpture, there is little doubt that eggs of the *II/c* eggshell morphotype were laid by a third crocodilian species. Furthermore, *II/a* and *II/c* are unique among all known extant and fossil crocodilian eggshells in two different aspects. Whereas crocodilian eggs in general have smooth or slightly undulating shell surface with shallow depressions and low ridges or nodes (Hirsch and Kohring 1992; Antunes et al. 1998; Carpenter 1999; Novas et al. 2009; Marzola et al. 2015), specimens of *MTII/a* with no incubational erosion or other abrasion show extremely pronounced surface sculpture with some tubercles as high as the non-sculptured thickness of the eggshell (Fig. 8E). The uniqueness of *MT II/c* lies in its extreme thinness (~90–130 μm) making it the thinnest crocodilian eggshell ever reported for any recent and fossil taxa (see Table 3 in Marzola et al. 2015 for comparison). Nevertheless, as is the case in some other fossil crocodilian eggs, thicknesses of *II/a* and *II/b* are also below the reported eggshell thicknesses of extant crocodile eggs. Based on eggshell thickness and corresponding egg mass measured in extant crocodiles (Marzola et al. 2015), egg mass could be roughly estimated as ~30 g, ~25 g, and ~5–10 g for *II/a*, *II/b*, and *II/c*, respectively. However, egg shape, dimensions, and eggshell thickness seem to vary more in fossil crocodiles than in extant taxa (see Tables 2 and 3 in Marzola et al. 2015) making such estimations unreliable. At present, the fragmentary nature of the eggshells from Iharkút prevents any further conclusion on the size and other physical attributes of the crocodilian eggs.

Pneumatic features were only investigated in *II/a*, where pore density (2.6/mm^2) well exceeds that described in *Alligator mississippiensis* (0.05/mm^2), *Crocodylus mindorensis*, and *Paleosuchus palpebrosus* (both ~0.2/mm^2; Marzola et al. 2015). However, pore diameter in absolute measure (~22 μm) as well as relative to total eggshell thickness (1:10) is much less in *MT II/a* than in any of the latter extant taxa (100–130 μm; 1:4–5; Marzola et al. 2015). The reason for this considerable difference may lie in an allometric relationship between egg size and porosity and/or eggshell thickness and porosity, but can also imply differences in nest structure and hence physical conditions within the nest (Tanaka et al. 2015 and references therein).

MT III. The general microstructural aspects of *MT III* (Figs 10 and 11) are strikingly similar to the eggshells of *Troodon* (Hirsch and Quinn 1990; Varricchio et al. 2002; Jackson et al. 2010; referred to as "hypsilophodontid" by Hirsch and Quinn 1990) collected from the Campanian (Upper Cretaceous) formations of Montana and Alberta. Three-layered microstructure with similar thickness ratios among the layers, radiating crystallites in the barrel-shaped mammillary cones and prismatic PL with fine growth laminations, the EL composed of blocky crystals, simple pores running perpendicular to the shell surface, and the lack of eggshell ornamentation are all shared characters between *MT III* and *Troodon* eggshell. However, besides the obvious difference in absolute shell thickness (~260 μm in *MT III* vs. 800–1,100 μm in *Troodon*), *MT III* shows a much broader range of mammillary cone width (21–170 μm) compared with that of *Troodon* (110–160 μm). This difference reflects the irregularly aggregated mammillae in *MT III* which may be due to local aggregation of organic cores resulting in fusion of radiating crystal growth in the mammillae, as described in bird eggshells (Tyler and Fowler 1978). Furthermore, crystal blocks in the EL of *MT III* are vertical, whereas they exhibit a slight inclination of ~5°–8° in the eggshell of *Troodon*. Finally, pores are relatively wider in *MT III*, making up ~10% of total eggshell thickness, as opposed to ~5% observed in *Troodon* (Jackson et al. 2010). These differences, however, do not undermine the taxonomic implications of the prominent similarities referring to close phylogenetic affinities between the egg layer of *MT III* and *Troodon*. Thus, the egg layer of *MT III* was apparently a maniraptoran, most probably paravian dinosaur. Following Ar et al. (1979), the eggshell thickness of *MT III* suggests an egg mass of ~30–40 g; about the size of a hen egg which is the 10th of the estimated mass of *Troodon* eggs (Varricchio and Jackson 2004). This implies that the egg layer was a significantly smaller bodied paravian theropod than *Troodon*.

Based on the nesting structure, clutch arrangement, porosity pattern, and the overall low water vapor conductance calculated for the eggs, *Troodon* was shown to have only partially buried its eggs in an otherwise open nest and that the adult incubated the largely exposed eggs (Varricchio et al. 2013). Keeping in mind the limitations of inferences due to the fragmentary nature of *MT III*, the listed common microstructural features of *MT III* and *Troodon* eggshells suggest similar, at least partially open-nest structure and possibly analogous incubation strategy in *MT III*. Although measurable pore density is higher in *MT III* than in *Troodon* eggshell (~0.7/mm^2 vs. ~0.1–0.3/mm^2),

the calculated density is based on a single CT-scanned fragment exhibiting two pore canals on its 2.87 mm^2 total surface area making pore density estimates uncertain at best. In the 13 specimens investigated by SEM and in thin section, only 2 pores could be positively identified, implying a general scarcity of pores in *MT III*. Nevertheless, if this density estimate proves to be representative of this eggshell type, the reported difference may still reflect allometric scaling relations between egg volume and pore density. In fact, estimated pore density in *MT III* corresponds to that in similar-sized bird eggs (Deeming 2006), which also supports an avian-like incubation strategy.

Rare morphotypes. The general morphology and microstructure of *MT IV* are reminiscent of those of the rigid eggshells of some extant gekkonids and fossil gecko-like eggshells (Hirsch et al. 1987; Hirsch and Harris 1989; Packard and Hirsch 1989; Kohring 1991; Mikhailov 1991; Packard and Demarco 1991) and that of the recently described fossil anguimorph egg (Fernandez et al. 2015). The most important shared characters are the nodular ornamentation and the single crystalline layer the shell units of which are formed of compact vertical columns with irregular, rugged outlines but lack mammillae. Despite the fact that the thickness of *MT IV* (~30–45 μm) fits the lowest range or falls even below the registered rigid eggshell thicknesses of most modern Gekkota species and other fossil lizards (~40–360 μm; Hirsch et al. 1987; Packard and Hirsch 1989; Hirsch 1996; Fernandez et al. 2015), its microstructure implies that *MT IV* is a rigid eggshell type. Similarly to the fossil anguimorph eggshell (Fernandez et al. 2015), *MT IV* has simple, non-branching vertical pore canals opening to the outer shell surface through the external protuberance, as opposed to the labyrinth-like network of interconnected channels in the crystalline layer of *Gekko* eggshell (Packard and Hirsch 1989). However, the single pore canal of *MT IV* available for description seems to retain or even expand its diameter within the crystalline layer, rather than exhibiting upside-down funnel shape with tapering canal in the mid-layer, as shown in the anguimorph lizard eggshell (Fernandez et al. 2015). Fine details of the crystalline pattern around the pore in *MT IV* cannot be observed; therefore, it cannot be compared with the pattern in the anguimorph eggshell. If *MT IV* was indeed of rigid type, based on known egg sizes and corresponding eggshell thicknesses in rigid-shelled lizard eggs (Hirsch et al. 1987; Fernandez et al. 2015), the egg size of *MT IV* could have been slightly smaller than that of the eggs of the recent gekkotan *Tarentola delalandii* (9 × 10 mm) and the Eocene fossil lizard egg (8 × 9 mm) from the Wind River Formation of Wyoming (Hirsch et al. 1987).

The single specimen of *MT V* discovered by thin sectioning lacks shell ornamentation and exhibits the so-called "ratite" type microstructure with a CL that characterizes the eggshell of extant and fossil paleognathous birds and other fossil maniraptoran dinosaurs, such as oviraptorids, the dromaeosaurid *Deinonychus*, enanthiornithine birds ("laevisoolithid" type), and some other "elongatoolithid" eggshell types of uncertain taxonomic identity but correlated with theropod dinosaurs (Hirsch and Quinn 1990; Norell et al. 1994; Zelenitsky et al. 1996, 2000; Mikhailov 1997; Zelenitsky and Hirsch 1997; Makovicky and Grellet-Tinner 2000; Schweitzer et al. 2002; Zelenitsky and Modesto 2003; Grellet-Tinner and Makovicky 2006;

Grellet-Tinner et al. 2006; Jin et al. 2007; Patnaik et al. 2009; Kurochkin et al. 2013; Huh et al. 2014). However, unlike oviraptorids which reveal only two structural layers, a ML and a continuous or squamatic layer (Norell et al. 1994; Zelenitsky et al. 1996; Grellet-Tinner et al. 2006; Weishampel et al. 2008), *MT V* has a trilaminate microstructure with a third, external zone, similar to extant paleognath birds (Zelenitsky et al. 1996; Mikhailov 1997; Zelenitsky and Modesto 2003) and fossil enantiornithines (Schweitzer et al. 2002; Kurochkin et al. 2013). Both the total eggshell thickness and the relative thickness of the three layers in *MT V* are approximately the same as described for the shells of enantiornithine bird eggs recovered from the Campanian (Upper Cretaceous) Río Colorado Formation, Argentina (Schweitzer et al. 2002). Furthermore, similar to the smooth surface of enantiornithine eggs (Schweitzer et al. 2002; Kurochkin et al. 2013), the preserved part of the single specimen of *MT V* reveals no ornamentation even in form of slight surface undulation that is so characteristic in oviraptorid eggshells (Norell et al. 1994; Grellet-Tinner et al. 2006; Weishampel et al. 2008). The preserved part of the mammillae in *MT V* lacks acicular crystal arrangement; it only shows long, slender, and parallel vertical prisms, similar to that demonstrated in the ML of *Porituberoolithus* (Fig. 3B, C in Zelenitsky et al. 1996; Fig. 2C, D in Tanaka et al. 2011) and an elongatoolithid eggshell (ZPAL MgOv-I/2) from the Maastrichtian (Upper Cretaceous) Nemegt Formation of Mongolia (Pl. 14/2 in Sabath 1991). As the single fragment of *MT V* does not show any pores, comparisons and inferences based on any aspects of porosity is not possible. Based on the similar shell thickness and microstructure, *MT V* is estimated to have belonged to an egg of similar dimensions as the enantiornithine *Gobipipus* eggs (4 × 2.5 cm; Kurochkin et al. 2013), about the size of hen eggs.

Potential egg layers among the fossil vertebrates of Iharkút

Vertebrate fossil assemblages do not give a complete record of diversity that once characterized the original community; therefore, the occurrence of cryptic taxa is to be expected (Behrensmeyer et al. 1979; Kidwell and Flessa 1996; Moore and Norman 2009). Even though eggshell fragments are not ideal fossils to expand our knowledge on amniote faunal composition, eggshells can be transported in the water a long distance from the original nesting sites (Hayward et al. 2011) and thereby may reveal a higher abundance (or maybe even presence of new) taxa in the local fauna that may not be reflected as such in the body fossil assemblage. For instance, if the main habitat of a species was farther away from the fluvial system, whereas its nesting site was close to it, eggshell fragments and skeletal remains can suggest different abundance relations or even presence/absence of a species.

On the basis of eggshell structure, thickness, and estimated egg size, the most frequent *MT I* is referable to a small-bodied theropod dinosaur, possibly about the size of a dove or a crow; thus, one might expect to find skeletal remains of such small theropods with relatively high frequency as well. However, as in other localities of

similar taphonomic conditions and paleoenvironment (e.g., Lauters et al. 2008; Britt et al. 2009), body fossils of small theropods are generally scarce in Iharkút, the terrestrial vertebrate assemblage of which is dominated by remains of ornithischian dinosaurs, most importantly the ankylosaur *Hungarosaurus* (83% of total dinosaur fossils; Ősi 2005; Botfalvai et al. 2015). Unfortunately, there is no reliable comparative eggshell material available at present for ankylosaurs or any ornithischian dinosaurs other than *Maiasaura* (Horner 1999), *Saurolophus* (Dewaele et al. 2015), and possibly *Telmatosaurus* (Grigorescu 2010) which, however, show entirely different eggshell microstructure from that observed in *MT I*. *Cairanoolithus* eggshells which were tentatively attributed to non-ornithopod ornithischians, possibly even ankylosaurs, by Sellés and Galobart (2016) are similar to *Maiasaura* eggshells in many respects but clearly distinct from *MT I*. Furthermore, pure dimensions of *Hungarosaurus* (~4–5 m length, ~650 kg; Ősi and Makádi 2009) or even those of *Struthiosaurus* (~2–3 m length, 300–400 kg; Pereda-Suberbiola 1992), the other recognized ankylosaur taxon in Iharkút (Ősi and Prondvai 2013), exceed the expected body mass of the egg layer of *MT I* by at least two magnitudes. Even though some dinosaurs, such as *Maiasaura* and the saurischian sauropods in general, are known from their curiously small eggs relative to their estimated adult body sizes (Horner 1999; Sander et al. 2011), based on the reconstructed relationship between pelvic aperture and egg size in *Struthiosaurus* (Sellés and Galobart 2016), much larger eggs with multiple times thicker eggshells than *MT I* are expected for the Iharkút ankylosaurs. Other ornithischians, such as the rhabdodontid *Mochlodon vorosi* (Ősi et al. 2012b) and the ceratopsian *Ajkaceratops kozmai* (Ősi et al. 2010a), are much rarer in Iharkút and still considerably larger than what would be expected of the egg layer of *MT I*. Thus, despite their high abundance in the skeletal material matching the high frequency of *MT I*, ornithischian dinosaurs are implausible candidates for the parent taxon of *MT I*. On the other hand, of the three non-avian theropod taxa identified at Iharkút, a 4–5-m-long basal tetanuran, a 1–2-m-long abelisaurid, and the chicken to turkey-sized *Pneumatoraptor fodori* (Ősi et al. 2010b), only *Pneumatoraptor* fits the estimated size range of the egg layer of *MT I*. Apart from these non-avian theropods, enantiornithine birds and indeterminate avian bones are also known from the locality, representing a size range from a sparrow-sized bird to the buzzard-sized enantiornithine *Bauxitornis mindszentyae*, although remains of the former may belong to a juvenile (Ősi 2008; Dyke and Ősi 2010). However, eggshells attributable to enantiornithines (Schweitzer et al. 2002; Kurochkin et al. 2013) have different structural features from those of *MT I*. Thus, the most parsimonious assumption is that *MT I* eggs were laid by a non-avian maniraptoran, possibly *Pneumatoraptor* or a similar sized, yet indeterminate taxon. However, the avian origin of *MT I* cannot be excluded. Porosity characteristics of the *MT I* eggshells point to buried nest conditions which suggest that even if the egg layer of *MT I* was avian, the nest was probably built on the ground. This, combined with the scarcity of adult body fossils, implies that parents did not incubate their eggs and that parental care may have been limited.

As in *MT I*, eggshell characteristics and estimated egg size of the much rarer *MT III* and the single specimen of *MT V* imply small-bodied non-avian or avian theropod egg layers. However, the microstructure of *MT III* is more comparable to that seen in extant neognath birds than that of *MT I*. Furthermore, as opposed to *MT I*, the inferred larger-sized eggs of *MT III* were most probably only partially buried or not buried at all in the nest, suggesting that the eggs were incubated by the parent animal(s), suggesting a higher level of parental care than that proposed for *MT I*. Thus, eggshell microstructure and inferred nesting strategy are more bird-like in *MT III* than in *MT I,* implying stronger avian affinities for *MT III*. Similarly, *MT V*, the thickest eggshell type from Iharkút, shows characteristics that relate it to a maniraptorantheropod, including any of the enantiornithine or other birds that might have inhabited the ancient fluvial environment of Iharkút. Even though the available data on this morphotype are admittedly very limited, we prefer to relate *MT V* to birds based on the frequent occurrence of similar microstructure in avian eggshells.

The three different subcategories of *MT II* refer to three different crocodilian egg layers, an inference which is in line with the abundance and diversity of crocodylomorph taxa known from the locality. Even though *MT II/a* and *II/b* were not initially separated for relative abundance quantification, *MT II/a* seems more abundant than *II/b*, and *II/c* is undoubtedly the rarest crocodilian eggshell type. Two of the four crocodilian taxa described from Iharkút, *Doratodon carcharidens* and the *Theriosuchus*-like crocodile, are very rare finds and were most likely terrestrial forms, whereas the two more common taxa, *Iharkutosuchus makadii* and *Allodaposuchus* sp., had semi-aquatic lifestyles (Ősi et al. 2007, 2012a; Rabi and Sebők 2015). Even though no direct evidence suggests such a relationship, based on relative abundances and habitat preference, *MT II/a* and *II/b* may have belonged to *Iharkutosuchus* and *Allodaposuchus*.

MT IV is most likely attributable to the rigid eggs of a squamate; a group of sauropsids exhibiting moderate diversity in the locality being represented by skeletal remains of four determinable and four indeterminate taxa of small-bodied terrestrial lizards and the freshwater mosasaur *Pannoniasaurus inexpectatus* (Makádi 2006, 2013a, 2013b; Makádi et al. 2012). As even basal mosasaurs were shown to have been live-bearing (Caldwell and Lee 2001; Field et al. 2015), and because of the extreme thinness and hence inferred small egg size of *MT IV*, the hypothesis that *MT IV* belonged to *Pannoniasaurus* can be discarded. The other four lizard taxa recovered from Iharkút, *Bicuspidon* aff. *hatzegiensis*, *Pelsochamops infrequens*, *Distortodon rhomboideus*, and *Chromatogenys tiliquoides* (Makádi 2006, 2013a, 2013b; Makádi and Nydam 2015), and the other, yet undescribed scincomorphs (Makádi pers. comm. 2016) are all outside of Gekkota, the only extant squamate clade where rigid shelled eggs occur (Pike et al. 2012). As for fossils, however, the rigid shelled egg with *in ovo* embryonic remains of an anguimorph lizard demonstrated that occurrence of rigid eggshell among fossil squamates cannot be restricted to Gekkota (Fernandez et al. 2015). Therefore, *MT IV* could be attributed to any of the aforementioned scincomorph taxa or to other, yet unknown squamates.

Comparison with other Late Cretaceous European eggshell localities

Besides the lack of complete eggs and embryonic remains in Iharkút, the composition and abundance distribution of eggshell morphotypes in the assemblage also differs from those of other Late Cretaceous eggshell-bearing localities of Europe: the Maastrichtian localities of the Haţeg Basin and Transylvania, Romania (Grigorescu et al. 1990, 2010; Codrea et al. 2002; Grigorescu and Csiki 2008; Grigorescu 2010; Csiki-Sava et al. 2015, 2016), the Campanian–Maastrichtian localities in southern France (Kerourio 1981, 1987; Garcia 2000; Garcia and Vianey-Liaud 2001; Vianey-Liaud et al. 2003; Vila et al. 2011), and the southern Pyrenean region in Spain (e.g., López-Martinez et al. 2000; López-Martínez et al. 2001; Vila et al. 2011; Sellés et al. 2013, 2014; Bravo and Gaete 2015). However, these latter localities comprise several meters of fossil-bearing strata, as opposed to the ~50- and ~30-cm thick layers in Unit 1 and SZ-7–8 in Iharkút. This difference in captured time range has to be kept in mind when comparing compositional and proportional distribution of eggshell types among these localities.

The fine-grained fluvio-lacustrine deposits in the Romanian localities have yielded mostly thick shells of megaloolithid eggs traditionally assigned to titanosaurian sauropods but recently considered to belong to the ornithopod *Telmatosaurus* in the Haţeg Basin (Grigorescu et al. 1990, 2010; Codrea et al. 2002; Grigorescu and Csiki 2008; Grigorescu 2010; Csiki-Sava et al. 2015, 2016). Furthermore, a drowned nesting colony of enantiornithine birds with eggshells of matrix-forming quantities (Dyke et al. 2012), thin "geckoid" shells with widespread occurrence but lower quantities, and prismatic theropod eggshells that appear to be the rarest finds (Csiki et al. 2008; Grigorescu and Csiki 2008; Vasile and Csiki 2011; Csiki-Sava et al. 2015, 2016) are also known from these localities. Based on the presented similarities with *MT I*, the "geckoid" eggshells are considered here as most likely belonging to theropod dinosaurs. The presence of turtle and crocodile eggshells is also mentioned in two abstracts only (Garcia et al. 2002, 2009) and no detailed publication supports these statements. Thus, at present only dinosaurian eggshell types are demonstrated from these Romanian localities.

The eggshell assemblages recovered from the Campanian–Maastrichtian lagoonal, fluvial, lacustrine, and marshy deposits of southwestern Europe are clearly dominated by megaloolithid eggshells to such extent that the different *Megaloolithus* oospecies are used for dating dinosaur fossil sites (Garcia and Vianey-Liaud 2001; López-Martínez 2003; Vila et al. 2011; Sellés et al. 2013; Sellés and Vila 2015). Nevertheless, other dinosaurian eggshell types assigned to ornithopods (spheroolithid types), theropods (prismathoolithid, ornithoid, ratite, laevisoolithid, elongathoolithid, and the oogenus *Pseudogeckoolithus*), and possibly to ankylosaurids (cairanoolithid types) are also very frequent finds in these localities (Garcia 2000; López-Martínez et al. 2001; López-Martínez 2003; López-Martínez and Vicens 2012; Sellés et al. 2013, 2014; Sellés and Vila 2015; Sellés and Galobart 2016). Whereas crocodilian eggshells were found in French as well as Spanish sites (Kerourio 1987; Garcia 2000;

Moreno-Azanza et al. 2014), turtle eggshells have been reported to date only from France (Garcia 2000). Because of our reinterpretation of the French "geckonoid" eggshells as representing the same theropod type as the oogenus *Pseudogeckoolithus*, no unambiguously squamate eggshells are known from these southwestern European localities.

The prevalence of megaloolithid eggs and eggshells in the Late Cretaceous Romanian and southwestern European localities is in sharp contrast with the complete absence of megaloolithid and other types of spherulitic dinosaurian eggshells at Iharkút. This, along with the overwhelming dominance of the theropod eggshell *MT I* in Hungary, clearly shows that the taxonomic composition and abundance distributions of the different egg layers at Iharkút are considerably different from any of the European Late Cretaceous eggshell localities. Unfortunately, insufficient descriptions of all non-megaloolithid eggshells from Romania hamper comparisons of possible taxonomic compositions. For instance, the single SEM image of an enantiornithine eggshell from the nesting colony provided by Dyke et al. (2012) does not reveal fine microstructural characteristics. However, the radial view appears to show gross morphological features not observed in any of the Iharkút morphotypes. Similarly, insufficient documentation of microstructural characteristics prevents proper comparison of the Romanian "geckoid" and prismatic theropod eggshell types with the eggshells from Iharkút. Nevertheless, it is highly likely that the widespread "geckoid" eggshells from Romania, the "geckonoid" eggshells from France, and the oogenus *Pseudogeckoolithus* from Spain and France originate from closely related, if not the same theropod taxon as *MT I*, and hence may represent a common element of these European Mesozoic eggshell assemblages. By contrast, *MT III* and *MT V*, the other two recognized dinosaurian eggshell types from Iharkút, do not show such close similarities with any of the well-documented southwestern European theropod eggshells, and hence may originate from endemic egg layers. *MT II/a*, *b*, and *c*, the three crocodilian eggshell types recovered from Iharkút also reveal unique features separating them from the crocodilian eggshells reported from France and Spain. Except for the comparatively thin (210–380 μm) crocodilian eggshells described from La Neuve, France (Garcia 2000), all *MT II* subcategories are considerably thinner (total range 90–240 μm) than the other Late Cretaceous crocodilian eggshells known from Europe (≥600 μm; Kerourio 1987; Moreno-Azanza et al. 2014). Even though eggshells from La Neuve have comparable thickness to *MT II/a* and *II/b*, they show a smooth outer surface as opposed to the prominent ridges in *MT II/a* and the moderate pits and elevations in *MT II/b*. These differences make a common egg layer taxon quite unlikely. Finally, *MT IV* is unparalleled by any other described eggshell types from the European Late Cretaceous having true squamate-like microstructure and extreme thinness. At present, turtle eggshells are not known from Iharkút.

Quantitative analyses

Quantitative analyses of eggshell structural characters showed that the prior qualitative classification of different morphotypes is reliable. Furthermore, these quantitative methods have proven to be adequate tools to distinguish structurally very similar eggshell types, such as the subcategories of *MT II*, which have subtle but statistically consistent differences. Finally, such multivartiate analyses can provide useful, independent complementary methods for general cladistic analyses of eggshells in future studies.

μXRF

Previously, Kocsis et al. (2009) performed an extensive geochemical survey of the Iharkút fossil assemblage using analyses of isotope ratios of O and Sr, and elemental abundances of REE, Fe, U, etc., in the bioapatite of bones and teeth of different aquatic and semi-aquatic vertebrates. Besides showing that Iharkút was a freshwater habitat, they found consistently high REE concentrations in the fossils, related to early diagenetic recrystallization. By contrast, we found generally low amounts or absence of REE and some other trace elements in the eggshell material. This may partially be due to the different measurement techniques applied in the two studies, but it likely also reveals genuine differences in the diagenesis of bone, teeth, and eggshells. Accumulation of REE and other trace elements occurs mostly when the organic content of the biological structure decays and authigenic apatite crystals accompanied by secondary minerals refill the vacant intercrystalline spaces as well as the original pore spaces (Trueman and Tuross 2002). Since bones and teeth have higher organic content and porosity than the calcitic layer of the eggshells, fossil skeletal elements are expected to reveal higher amounts of REE and trace elements than the preserved calcareous parts of eggshells. Differences in composition of the mineral phase (hydroxylapatite vs. calcite/aragonite) may also play a role in a different diagenesis, considering the general susceptibility of calcite to diagenetic alteration (Mackenzie 2014). The highest abundance of trace elements and resin-glue compounds in one of the *MT I* specimens (Fig. 21) implies that this fragment may have had higher original porosity, which facilitated the accumulation of secondary minerals during early diagenesis as well as enabled the embedding resin components to seep through the pores of the eggshell. This interpretation is in line with the observation that *MT I* shows the highest porosity among the three major morphotypes in both number and relative diameter of pores piercing through the entire eggshell thickness.

The translucent/glassy appearance under macro- and microscopic view of the single scanned specimen of *MT II/c* (Fig. 14) suggests that it could have experienced a different diagenetic setting compared with the other specimens. This is supported by the PCA results of the spectral data (Fig. 21I) which places this *MT II/c* fragment

farther from the central group of specimens on the PC1–PC2 plot. Despite the obvious difference in appearance compared with all other opaque fragments showing the general brownish coloration and its slightly offset position on the PC1–PC2 plot, no prominent compositional difference could be detected in this specimen.

The high amount of phosphorous revealed in the ML of a specimen from category *MT III* deserves further consideration. The spatial restriction of the P-peak to the mammillae suggests that the high P-content may be related to the originally high organic content of this area. In a recent study, eggshell membrane of hen eggs was used as a medium to artificially grow hydroxylapatite (calcium phosphate) minerals (Li et al. 2011; Zhang et al. 2011). Francolite, a carbonate-rich variety of hydroxylapatite, has also been shown to precipitate in organic matter-rich carbonates under anoxic conditions (Tribovillard et al. 2010). Since anoxic conditions prevailed during early diagenesis of the Iharkút fossil assemblage (Kocsis et al. 2009), the high amount of P in this particular *MT III* fragment may represent remnants of phosphatized organic cores or fibers of the eggshell membrane in which the mammillae were originally anchored. Nevertheless, no definite eggshell membrane remains are preserved in any of the fragments.

Taphonomic and paleoecological implications

River floodplains are known to be ideal preservational environments for eggshells where rapid burial produces rich eggshell horizons in the alluvial sediments (Paik et al. 2004; Liang et al. 2009; Oser and Jackson 2014; Venczel et al. 2015). To understand the physical and/or chemical processes facilitating eggshell preservation, the sedimentological and taphonomic investigation of these fluvial deposits are indispensable (Hayward et al. 2000, 2011; Clayburn et al. 2004; Liang et al. 2009; Jackson et al. 2013; Oser and Jackson 2014). Detailed taphonomic study of the Iharkút vertebrate locality has already been carried out on the basis of skeletal material (Botfalvai et al. 2015). Nonetheless, the preservation of eggshell fragments adds to our knowledge of the depositional environment of the two different sites, Unit 1 and SZ-7–8, which were concentrated by different fluvial processes.

Unit 1, which yielded the vast majority of the eggshell assemblage (~40 fragments/kg residue), represents episodic high-density flash-flood deposits (Botfalvai et al. 2015, 2016), implying that the eggshell fragments were transported by high-energy currents. Most of the eggshells are well preserved with distinct ornamentation, but several samples display moderate edge wear which may indicate short-term (maximum 1 week) tumbling and erosion (Oser and Jackson 2014), whereas a small percentage of shells (<8%) shows a higher degree of surface abrasion. These differences in the degree of abrasion may point to differences in the length of transportation or other type of exposure to physical erosion (Behrensmeyer 1982; Behrensmeyer et al. 1986; Aslan and Behrensmeyer 1996; Zeigler 2005; Britt et al. 2009). The fact that about 80% of the fragments are well preserved suggests that these eggshells were collected from the floodplain environment not far from the site of

deposition and were transported above the channel surface by turbulent currents of a high-density flow only for a short period. Short transport of these fragments is also supported by the findings of a natural stream experiment where smaller eggshell fragments were shown to be transported for shorter distance than larger pieces which have greater surface area and concavity to be pushed along in the stream (Hayward et al. 2011). In line with the sedimentological conclusions (Botfalvai et al. 2016), the eggshell fragments may have been deposited when the current velocity suddenly decreased and silt began to accumulate from the standing water following the flow events. The presence of eggshell fragments in the basal breccia layer of Unit 1 also confirms the hypothesis (Botfalvai et al. 2015, 2016) that this depositional environment was a trapping place with sudden drop in current velocity (Behrensmeyer 1975; Moore and Norman 2009) that allowed simultaneous accumulation of particles of very different densities (e.g., bones, plants, and eggshells) and sizes (from microfossils to partial ankylosaur skeletons).

By contrast, site SZ-7–8, which to date has yielded only five eggshell fragments (~2.5 fragments/kg residue), consists of dark gray siltstone and clay (Botfalvai et al. 2016). Its depositional environment was characterized by overall hydromorphy and oxygen-poor conditions at the time of accumulation as well as during early diagenesis because (1) this facies shows a close association with the hydromorphic paleosols and the sheet sandstone bodies (crevasse splay deposit); (2) it shows relatively high concentration of pyrite which forms a crust around mollusk shells and bones; (3) it preserves high organic content in form of coalified plant material; features generally characterizing reducing, water-saturated environments (Davies-Vollum and Wing 1998; Kraus 1999; Retallack 2001; Therrien 2005; Roberts 2007). Pollen remains of fossil plants such as *Triatriopollenites* associated with Myricaceae known from this layer (Bodor and Baranyi 2012) also indicate a swampy environment (Akkiraz et al. 2008). Finding well-preserved calcitic eggshell fragments in such deposits is uncommon: whereas fossil eggs and eggshell fragments are frequently recovered from well-drained, reddish, carbonate-rich paleosols (e.g., Paik et al. 2004; Van Itterbeeck et al. 2004; Grigorescu and Csiki 2008; Liang et al. 2009; Jackson et al. 2013; Venczel et al. 2015), only sporadic occurrences are known from similar water-logged environments (López-Martinez et al. 2000; Hastings and Hellmund 2015). The rarity of eggshells in deposits of stagnant, poorly oxygenated pools of swampy floodplain environments is usually explained by the unfavorable conditions related to high acidity which is induced by the anaerobic decay of plant material and dissolves calcareous eggshells in a short amount of time (Retallack 1984; Hayward et al. 1991; Clayburn et al. 2004; Bailey et al. 2005). The fine preservation of the eggshells recovered from site SZ-7–8 thus indicates that the depositional environment could not have been very acidic despite the high organic content and most likely high concentrations of humic acids derived from the anaerobically decaying plant remains. Therefore, it is reasonable to assume the presence of a chemical buffer that neutralized the acidic conditions characterizing such environments and allowed preservation of the calcareous eggshells. Such a buffering effect could have originated from the catchment bedrock and

surficial sediments, the geology and composition of which are known to play an important role in determining local chemical attributes (Bailey et al. 2005). The Iharkút locality was situated on an uplifted Mesozoic carbonate block in the Transdanubian Range during the Late Cretaceous (Jocha-Edelényi 1988; Mindszenty et al. 2000) where parallel-running limestone mountain ridges and other elevated areas separated the valleys also underlain by calcareous bedrock (Tari 1994). Furthermore, the sediments deposited in the Iharkút section are composed primarily of dolomite, quartz pebbles, and clay clasts bound by calcareous cement. Because alkalinity is largely determined by the carbonate ions originating mostly from the weathering of local bedrock (Bailey et al. 2005), the geology of the Iharkút depositional environment suggests that the alkalinity of surface water and groundwater was probably considerable and could have compensated for the acidity originating from the anoxic decomposition of plant material (Bailey et al. 2005). Therefore, we suggest that this buffering capacity of carbonate-rich water enabled the preservation of eggshells in the initially unfavorable, water-saturated swampy environment. Even though it has been shown experimentally that all water solutions, including those with alkaline pH, have considerable corrosive effect on eggshells (Clayburn et al. 2004), other factors influencing eggshell corrosion (e.g., temperature, time of exposure to moisture) are unknown characteristics of SZ-7–8. The preservation of eggshells with distinct surface ornamentation indicates that these undefined factors were less damaging, although shell fragmentation into few square-millimeter pieces already rates as significant corrosion of the original shell and may have been partially evoked by the water-saturated conditions. The presence of coarser particles (fine-grained sand) in the massive dark siltstones of SZ-7–8 suggests that the area had clastic input by low energy currents (Botfalvai et al. 2015, 2016). Transport of the eggshell material was probably negligible or limited to short ranges when rainfall induced episodic water flows which may have collected parautochthonous particles from the surrounding area into the small-scale stagnant pools.

Considering the faunal composition and relative abundances of different taxa based on skeletal material recovered from Iharkút, the unexpected predominance of the theropod eggshell *MT I* providing 83% of the total weight of the eggshell assemblage needs further attention. Such preponderance in Unit 1 cannot be explained by the local burial of a single nest, as relative abundances of different eggshell morphotypes are consistent across all material that were grouped by a year of collection and collected from more than 165 m^3 of fossiliferous sediments corresponding to ~550 m^2 excavated area throughout 15 years of excavation. Furthermore, the lack of complete eggs and embryos also argues against *in situ* burial of a single nest or nesting colony. Positive preservational bias of *MT I* relative to the other eggshell morphotypes is also unlikely, since *MT I* is the thinnest and hence the most fragile of the three common eggshell morphotypes. Based on sedimentological and taphonomic characteristics of Unit 1 (Botfalvai et al. 2015, 2016), any sorting effect preferentially accumulating *MT I* is also implausible. Finally, the few eggshells recovered from SZ-7–8 all represent *MT I*, despite the considerable differences in inferred depositional

environments between SZ-7–8 and the major fossiliferous site, Unit 1. All these factors imply that high abundance of *MT I* in the eggshell assemblage reflects true prevalence of *MT I* nests in the alluvial plain environment of the river system. As Unit 1 was probably deposited over a very short time due to a rapid sequence of flash-flood events, therefore, it may represent only a snapshot of abundance relationships that are not necessarily representative of long-term community patterns. However, the exclusivity of *MT I* in the most likely autochthonous assemblage of SZ-7–8 [the layers of which were deposited in stagnating water for a much longer period than those of Unit 1 (Botfalvai et al. 2016)] argues against the hypothesis that the dominance of *MT I* in the more allochthonous assemblage of Unit 1 is merely an incidental, short-term concentration of this morphotype during the flash-flood events. Therefore, it is well supported that *MT I* was indeed the dominant eggshell type in the low-level floodplain environment reconstructed for the locality. The overwhelming majority of *MT I* in the eggshell assemblage, in contrast with the underrepresentation of skeletal remains of small-bodied non-avian and avian theropods, supports the hypothesis that the population of egg layers lived farther away from the river system, while their nesting site was close to or within the topographically low-lying, wet, floodplain areas.

A further taphonomic peculiarity is the complete lack of aragonitic turtle eggshells which is in sharp contrast with the high abundance of turtle skeletal remains known from the locality (Botfalvai et al. 2015). Aragonite is a less stable crystalline phase of calcium carbonate than calcite, is more prone to dissolution in slightly acidic environments, and tends to alter to calcite on a geologic time scale (Retallack 1984; Tucker and Wright 1990). Since calcite is known to form the eggshells of all amniotes except for turtles (Mikhailov 1991), the instability of the aragonite phase explains the lack of turtle eggshells in the assemblage. However, gastropod shells, which are originally also composed of aragonite (Flügel 2010), are relatively abundant in the same fossiliferous layers. Even if the original aragonitic gastropod shells had been recrystallized into calcite, the question remains why turtle eggshells, if present in the ancient environment, were not preserved the same way. Turtles generally bury their eggs in moist sand or other type of wet soil (Witt and Caldwell 2004), so the implied fluvial environment seem to be ideal nesting site for turtles, making the absence of turtle eggshells even more puzzling. Since different extant turtles exhibit an astonishing diversity in the physical properties of their eggshells (Kusuda et al. 2013), a possible explanation could be that the most abundant turtle known from the locality, the aquatic bothremydid *Foxemys trabanti* (Rabi et al. 2011), laid soft-shelled eggs, as do numerous living turtles today. The potentially soft nature of turtle eggshells may account for their absence in the fossil record, since the depositional environment of Iharkút is clearly not favorable for preservation of soft tissues. As for now, however, it remains uncertain whether their lack is genuine and turtles did not nest on the alluvial plains of the river system or whether it is a taphonomic bias relating to the low preservation potential of possibly soft eggshells.

Unique features of the Iharkút eggshell assemblage

The taxonomic composition and diversity are notable but not the most intriguing features of the eggshell assemblage recovered from the Santonian layers of Iharkút. Rather, its unprecedented characteristics are the presence of the thinnest recorded eggshells of their kinds and the exclusiveness of thin eggshells (≤300 μm) in this assemblage, as compared with those described from other fossil localities. Among these eggshells, we report the thinnest crocodilian (*MT II/c*) and rigid squamate (*MT IV*) eggshells ever described from the fossil record. In fact, *MT II/c* and *MT IV* represent the thinnest calcareous eggshells even among the extant, rigid-shelled members of their respective taxonomic groups for which calcareous eggshell thicknesses have been reported to date (Hirsch et al. 1987; Hirsch 1996; Moreno-Azanza et al. 2014; Fernandez et al. 2015; Marzola et al. 2015). *MT I* is also among the thinnest known Mesozoic theropod eggshells, matching the thinness of the thinnest known fossil avian eggshells (Sabath 1991; Schweitzer et al. 2002; Fernández et al. 2013; Kurochkin et al. 2013; Zhang et al. 2015). Although it is most likely that such thin eggshells would be more frequent finds in any other localities if systematic screen-washing were widely used besides *in situ* recognition and excavation of fossils, the complete lack of thick eggshells is still a peculiarity of the Iharkút eggshell assemblage. The absence of thick eggshells cannot result from a negative bias in their fossilization potential, nor can it be explained by sorting in the depositional environment (Botfalvai et al. 2015, 2016). Even though the currently known terrestrial amniote fauna of Iharkút is composed of small to medium-sized animals (≤650 kg; Ősi and Makádi 2009; Ősi et al. 2012a) which may relate to island conditions (but see Ősi et al. 2012b), reasonable egg size estimation for the larger non-avian dinosaur taxa (all ornithischians, abelisaurid, and tetanuran theropods) well exceeds the egg size estimated for the thickest recovered eggshells. Hence, it is highly likely that these taxa laid their presumably much larger eggs in areas farther away from the river system which otherwise could have collected and deposited their eggshells. By contrast, the abundance of thin eggshells refers to the nesting preference of small-bodied sauropsids close to the alluvial plains.

The revealed segregation of nesting sites between small and medium to larger-bodied dinosaurs may provide further insights into the paleoecology of the Iharkút terrestrial fauna. For instance, the abundance of *Hungarosaurus* remains and the presence of multiple partial skeletons exclusive for this taxon in the locality, support the hypothesis that wetland areas represented the habitat of *Hungarosaurus* (Botfalvai et al. 2015), as assumed for ankylosaurs in general (Horner 1979; Lee 1996; McCrea et al. 2001). This clearly implies a topographical and environmental separation of general habitat and nesting site for this taxon. Thus, *Hungarosaurus* lived and fed in the dense subtropical floodplain forests associated with the river system, whereas it laid its eggs farther away from the alluvial plains, for instance in the less dense forests of more elevated areas (Bodor and Baranyi 2012; Bodor et al. 2012).

Conclusions

Using a variety of visualization, explorative and quantitative techniques, we showed that the diverse and intriguing assemblage of eggshell fragments recovered from the Santonian beds at the Iharkút vertebrate locality contains eggshell types of three different theropod dinosaurians, three different crocodilians, and one probable squamate. These can be tentatively attributed to small-bodied members of the local fauna. As for the three dinosaurian types, *MT I*, *MT III*, and *MT V*, *Pneumatoraptor*, *Bauxitornis*, and/or other small-sized theropods or birds are the most likely egg layers. Even though *Iharkutosuchus* and *Allodaposuchus*, the most abundant crocodilian fossils in the locality, are candidates for laying the two most frequently found crocodilian eggshell types, *MT II/a* and *MT II/b*, there is no further evidence to support or reject these assignments. Thus, each crocodilian subcategory, *MT II/a*, *II/b*, and the scarcest *II/c* could have been produced by any of these two aquatic, or the other two, much rarer and terrestrial crocodilians known from Iharkút, a *Theriosuchus*-like form and *Doratodon*. The *MT IV* of squamatan affinity might have equally belonged to any of the terrestrial squamate taxa described from Iharkút. Of all the identified eggshell types, only *MT III* shows characteristics of having been laid in a half or fully open nest, whereas the others, with the possible exception of the poorly known *MT V*, were most likely buried in decaying detritus or soil.

Comparing the inferred taxonomic composition with other Late Cretaceous European eggshell assemblages, the theropod dinosaurian *MT I*, the most abundant eggshell type in Iharkút, seems to be a common element with other localities showing close resemblance to *Pseudogeckoolithus* from Spain, and the "geckoid" types from France and Romania where, however, these types were identified as having belonged to a squamate. The complete lack of megaloolithid and spheroolithid eggshells probably belonging to sauropods and ornithischian dinosaurs is a distinct compositional feature of the Iharkút eggshell assemblage as opposed to all other Late Cretaceous European localities yielding mostly such eggs and eggshells.

The Iharkút eggshell assemblage is unique for at least two other reasons. First, it is composed exclusively of eggshells not thicker than ~300–320 μm, even though most known dinosaurian members of the Iharkút fauna are significantly larger than the inferred body size of the egg layers based on eggshell thicknesses. Since no taphonomic effect could be identified as accounting for the lack of thicker eggshells in either of the investigated sites, we conclude that there was most probably a segregation in nesting site preferences of small and large-bodied taxa with the smaller ones nesting close to the fluvial system and the larger ones farther away from it. Second, this eggshell assemblage contains the thinnest crocodilian (*MT II/c*) and squamate (*MT IV*), and one of the thinnest Mesozoic theropod (*MT I*) eggshells reported to date. This may be explained by the general collection bias toward excavating larger fossil specimens that can be spotted and collected on site, as opposed to the rarity of long-term and systematic screen-washing activity, which yields most of these fragile, cryptic microfossils.

Chemical compositional differences were revealed among the eggshell fragments as well as between the eggshells of this study and a variety of skeletal material reported in an earlier study. For instance, the most porous eggshell type *MT I*, just like porous bones, is more prone to accumulate REE and trace elements than eggshells of lower porosity, while the original organic content in the robust mammillae of *MT III* seems to have initiated regional phosphate precipitation in the innermost eggshell layer. Hence, this variety may be explained by differences in original porosity, organic content, and mineral structure and composition of these biological materials, features that strongly influence the processes of early diagenesis of fossils.

Some taphonomic aspects of this assemblage are also noteworthy. Whereas Unit 1 yielding almost all but five eggshell fragments represents sequential flash-flood deposits favorable for eggshell preservation, SZ-7–8 was an oxygen-poor, water-logged, swampy environment of probably high humic acid content due to decaying plant material, which generally dissolves the calcareous eggshells in a short amount of time. Despite these acidic conditions unfavorable for eggshell preservation, this site also provided five well-preserved eggshell fragments. This suggests that water acidity derived from rotting plants was buffered by the carbonate-rich alkaline water solutions originating from the weathering of calcareous bedrock and sediments characterizing this locality. Finally, the overwhelming majority of *MT I* in Unit 1 and its exclusiveness in SZ-7–8, which represents a longer time interval in a quite different depositional environment, suggest the predominance of nests belonging to a small theropod dinosaur in this ancient habitat.

This study draws attention to the general importance of fossil collection by screen-washing which can reveal hidden diversity and abundance distribution of microfossils, such as eggshell fragments, and provide further insights into the paleoecological and taphonomic aspects of the fossil localities.

Acknowledgements

The authors would like to thank József Pálfy for his useful suggestions on an earlier version of this work. We are grateful to Réka Kalmár and Márton Szabó for technical assistance in thin sectioning and picking fossils from sediment residue, to Krisztina Buczkó for introducing and teaching SEM technique and helping with sample preparations, to Christina Makarona and Niels de Winter for instructions and help in μXRF operation and analysis, and to Orsolya Győri and Andrea Mindszenty for useful discussions on geology and sedimentology. We also would like to thank Lénárd Szabó, Zsolt Bencze, Zoltán Tar, and Tamás Földes for organizing beam time and performing μCT scanning. The following institutes are thanked for providing logistics and access to facilities: Department of Botany and Department of Paleontology and Geology, Hungarian Natural History Museum, Hungary; Department of Physical and Applied Geology and Department of Paleontology, Eötvös Loránd University, Hungary; Vrije Universiteit Brussel, Belgium; Continental Automotive Hungary Kft,

Hungary; Trigo Quality Control and Quality Services, Hungary. Research grants given to authors and supporting different phases of this study are as follows: Bijzonder Onderzoeksfond – Ghent University for EP (Grant no. 01P12815); National Geographic Society (Grant nos. 7228-02 and 7508-03), National Research, Development and Innovation Office (OTKA, Grant nos. PD 73021, NF 84193, and K116665), MTA Lendület Program (Grant no. 95102) for AŐ; Fonds voor Wetenschappelijk Onderzoek Vlaanderen (Grant no. 12L7115N) for KS.

References

Agnolin, F.L., J.E. Powell, F.E. Novas, M. Kundrát 2012: New alvarezsaurid (Dinosauria, Theropoda) from uppermost cretaceous of north-western Patagonia with associated eggs. – Cretaceous Research, 35, pp. 33–56.

Akkiraz, M.S., M.S. Kayseri, F. Akgün 2008: Palaeoecology of coal-bearing Eocene sediments in Central Anatolia (Turkey) based on quantitative palynological data. – Turkish Journal of Earth Sciences, 17/2, pp. 317–360.

Antunes, M.T., P. Taquet, V. Ribeiro 1998: Upper Jurassic dinosaur and crocodile eggs from Paimogo nesting site. – Memórias de Academia de Ciências de Lisboa, 37, pp. 83–99.

Ar, A., H. Rahn, C.V. Paganelli 1979: The avian egg: Mass and strength. – Condor, 81, pp. 331–337.

Aslan, A., A.K. Behrensmeyer 1996: Taphonomy and time resolution of bone assemblages in a contemporary fluvial system: The East Fork River, Wyoming. – Palaios, 11/5, pp. 411–421.

Bailey, J.V., A.S. Cohen, D.A. Kring 2005: Lacustrine fossil preservation in acidic environments: Implications of experimental and field studies for the Cretaceous–Paleogene boundary acid rain trauma. – Palaios, 20/4, pp. 376–389.

Behrensmeyer, A.K. 1975: The taphonomy and paleoecology of Plio-Pleistocene vertebrate assemblages east of Lake Rudolf, Kenya. – Bulletin of the Museum of Comparative Zoology, 146, pp. 473–478.

Behrensmeyer, A.K. 1982: Time resolution in fluvial vertebrate assemblages. – Paleobiology, 8/3, pp. 211–227.

Behrensmeyer, A.K., D. Western, D.E. Dechant Boaz 1979: New perspectives in vertebrate paleoecology from a recent bone assemblage. – Paleobiology, 5/1, pp. 12–21.

Behrensmeyer, A.K., K.D. Gordon, G.T. Yanagi 1986: Trampling as a cause of bone surface damage and pseudo-cutmarks. – Nature, 319, pp. 768–771.

Board, R.G., N.H.C. Sparks 1991: Shell structure and formation in avian eggs. – In: Deeming, C.D., M.W.J. Ferguson (Eds): Egg Incubation: Its Effects on Embryonic Development in Birds and Reptiles. Cambridge University Press, Cambridge, pp. 71–86.

Bodor, E., V. Baranyi 2012: Palynomorphs of the Normapolles group and related plant mesofossils from the Iharkút vertebrate site, Bakony Mountains (Hungary). – Central European Geology, 55, pp. 259–292.

Bodor, E., V. Baranyi, Z. He manová 2012: The earliest Sabiaceae fruit remains of Hungary. – Hantkeniana, 7, pp. 11–18.

Botfalvai, G., A. Ősi, A. Mindszenty 2015: Taphonomic and paleoecologic investigations of the Late Cretaceous (Santonian) Iharkút vertebrate assemblage (Bakony Mts, Northwestern Hungary). – Palaeogeography, Palaeoclimatology, Palaeoecology, 417, pp. 379–405.

Botfalvai, G., J. Haas, E. Bodor, A. Mindszenty, A. Ősi 2016: Facies architecture and palaeoenvironmental implications of the Upper Cretaceous (Santonian) Csehbánya formation at the Iharkút vertebrate locality (Bakony Mountains, Northwestern Hungary). – Palaeogeography, Palaeoclimatology, Palaeoecology, 441, pp. 659–678.

Bravo, A.M., R. Gaete 2015: Titanosaur eggshells from the Tremp Formation (Upper Cretaceous, Southern Pyrenees, Spain). – Historical Biology, 27, pp. 1079–1089.

Bravo, A.M., A.D. Buscalioni, L. Merino, G.B. Müller 2003: Experimental taphonomy of avian eggs and eggshells: Effects on early diagenesis. – Palaeovertebrata, 32, pp. 77–95.

Britt, B.B., D.A. Eberth, R.D. Scheetz, B.W. Greenhalgh, K.L. Stadtman 2009: Taphonomy of debris-flow hosted dinosaur bonebeds at Dalton Wells, Utah (Lower Cretaceous, Cedar Mountain Formation, USA). – Palaeogeography, Palaeoclimatology, Palaeoecology, 280, pp. 1–22.

Caldwell, M.W., M.S.Y. Lee 2001: Live birth in Cretaceous marine lizards (mosasauroids). – Proceedings of the Royal Society of London B, 268, pp. 2397–2401.

Carpenter, K. 1999: Eggs, Nests, and Baby Dinosaurs: A Look at Dinosaur Reproduction. – Indiana University Press, Bloomington, IN, 352 p.

Clayburn, J.K., D.L. Smith, J.L. Hayward 2004: Taphonomic effects of pH and temperature on extant avian dinosaur eggshell. – Palaios, 19/2, pp. 170–177.

Codrea, V., T. Smith, P. Dica, A. Folie, G. Garcia, P. Godefroit, J. Van Itterbeeck 2002: Dinosaur egg nests, mammals and other vertebrates from a new Maastrichtian site of the Haţeg Basin (Romania). – Comptes Rendus Palevol, 1/3, pp. 173–180.

Csiki, Z., A. Ionescu, D. Grigorescu 2008: The Budurone microvertebrate site from the Maastrichtian of the Haţeg Basin – Flora, fauna, taphonomy and paleoenvironment. – Acta Palaeontologica Romaniae, 6, pp. 49–66.

Csiki-Sava, Z., E. Buffetaut, A. Ősi, X. Pereda-Suberbiola, S.L. Brusatte 2015: Island life in the Cretaceous – Faunal composition, biogeography, evolution, and extinction of land-living vertebrates on the Late Cretaceous European archipelago. – ZooKeys, 469, pp. 1–106.

Csiki-Sava, Z., M. Vremir, S. Vasile, S.L. Brusatte, G. Dyke, D. Naish, M.A. Norell, R. Totoianu 2016: The East side story – The Transylvanian latest Cretaceous continental vertebrate record and its implications for understanding Cretaceous–Paleogene boundary events. – Cretaceous Research, 57, pp. 662–698.

Davies-Vollum, K.S., S.L. Wing 1998: Sedimentological, taphonomic, and climatic aspects of Eocene swamp deposits (Willwood formation, Bighorn Basin, Wyoming). – Palaios, 13/1, pp. 28–40.

Deeming, C.D. 2006: Ultrastructural and functional morphology of eggshells supports the idea that dinosaur eggs were incubated buried in a substrate. – Palaeontology, 49, pp. 171–185.

Deeming, C.D., M.W.J. Ferguson 1991: Egg Incubation: Its Effects on Embryonic Development in Birds and Reptiles. – Cambridge University Press, Cambridge, 448 p.

Dewaele, L., K. Tsogtbaatar, R. Barsbold, G. Garcia, K. Stein, F. Escuillié, P. Godefroit 2015: Perinatal specimens of *Saurolophus angustirostris* (Dinosauria: Hadrosauridae), from the Upper Cretaceous of Mongolia. – PLoS One, 10/10, p. e0138806.

Dyke, G., A. Ősi 2010: A review of Late Cretaceous fossil birds from Hungary. – Geological Journal, 45, pp. 434–444.

Dyke, G., M. Vremir, G. Kaiser, D. Naish 2012: A drowned Mesozoic bird breeding colony from the Late Cretaceous of Transylvania. – Naturwissenschaften, 99, pp. 435–442.

Ewert, M.A., S.J. Firth, C.E. Nelson 1984: Normal and multiple eggshells in batagurine turtles and their implications for dinosaurs and other reptiles. – Canadian Journal of Zoology, 62, pp. 1834–1841.

Fay, M. 2010: Exact or Asymptotic Permutation Tests. R Package 'perm'. – https://cran.r-project.org/web/packages/perm/index.html.

Ferguson, M.W.J. 1982: The structure and composition of the eggshell and embryonic membranes of *Alligator mississippiensis*. – Transactions of the Zoological Society of London, 36, pp. 99–152.

Fernández, M.S., R.A. Garcia, L. Fiorelli, A. Scolaro, R.B. Salvador, C.N. Cotaro, G.W. Kaiser, G. Dyke 2013: A large accumulation of avian eggs from the Late Cretaceous of Patagonia (Argentina) reveals a novel nesting strategy in Mesozoic birds. – PLoS One, 8/4, p. e61030.

Fernandez, V., E. Buffetaut, V. Suteethorn, J.C. Rage, P. Tafforeau, M. Kundrát 2015: Evidence of egg diversity in squamate evolution from cretaceous anguimorph embryos. – PLoS One, 10/7, p. e0128610.

Field, D.J., A. LeBlanc, A. Gau, A.D. Behlke 2015: Pelagic neonatal fossils support viviparity and precocial life history of Cretaceous mosasaurs. – Palaeontology, 58, pp. 401–407.

Flügel, E. 2010: Microfacies of Carbonate Rocks: Analysis, Interpretation and Application (2nd ed.). – Springer-Verlag, Berlin, Heidelberg, 984 p.

Garcia, G. 2000: Diversité des coquilles "minces" d'oeufs fossiles du Crétacé supérieur du Sud de la France (Diversity of fossil eggshell fragments from the Upper Cretaceous of southern France). – Geobios, 33/1, pp. 113–126.

Garcia, G., M. Vianey-Liaud 2001: Dinosaur eggshells as biochronological markers in Upper Cretaceous continental deposits. – Palaeogeography, Palaeoclimatology, Palaeoecology, 169, pp. 153–164.

Garcia, G., T. Smith, A. Folie, P. Godefroit, J. Van Itterbeeck, V. Codrea 2002: Parataxonomic classification of eggshells from Pui in the Haţeg Basin (Romania). – In: Grigorescu, D., Z. Csiki (Eds): 7th European Workshop on Vertebrate Palaeontology. Abstracts Volume and Excursions Field Guide. Sibiu, Romania, p. 13.

Garcia, G., P. Godefroit, T. Smith, J. Van Itterbeeck, X. Valentin, V. Codrea 2009: Amniotic eggshells from the Haţeg Basin (Upper Cretaceous, Romania). – In: Godefroit, P., O. Lambert (Eds): Tribute to Charles Darwin and Bernissart Iguanodons: New Perspectives on Vertebrate Evolution and Early Cretaceous Ecosystems. Darwin–Bernissart Meeting, Abstracts Volume, Brussels, p. 42.

Grellet-Tinner, G., P. Makovicky 2006: A possible egg of the dromaeosaur *Deinonychus antirrhopus*: Phylogenetic and biological implications. – Canadian Journal of Earth Sciences, 43, pp. 705–719.

Grellet-Tinner, G., L. Chiappe, M. Norell, D. Bottjer 2006: Dinosaur eggs and nesting behaviors: A paleobiological investigation. – Palaeogeography, Palaeoclimatology, Palaeoecology, 232, pp. 294–321.

Grigorescu, D. 2010: The "Tustea Puzzle": Hadrosaurid (Dinosauria, Ornithopoda) hatchlings associated with Megaloolithidae eggs in the Maastrichtian of the Haţeg Basin (Romania). – Ameghiniana, 47, pp. 89–97.

Grigorescu, D., Z. Csiki 2008: A new site with megaloolithid egg remains in the Maastrichtian of the Haţeg Basin. – Acta Palaeontologica Romaniae, 6, pp. 115–121.

Grigorescu, D., M. Şeclăman, D.B. Norman, D.B. Weishampel 1990: Dinosaur eggs from Romania. – Nature, 346, p. 417.

Grigorescu, D., G. Garcia, Z. Csiki, V. Codrea, A.V. Bojar 2010: Uppermost Cretaceous megaloolithid eggs from the Haţeg Basin, Romania, associated with hadrosaur hatchlings: Search for explanation. – Palaeogeography, Palaeoclimatology, Palaeoecology, 293, pp. 360–374.

Grine, F.E., J.W. Kitching 1987: Scanning electron microscopy of early dinosaur egg shell structure: A comparison with other rigid sauropsid eggs. – Scanning Microscopy, 1, pp. 615–630.

Hastings, A.K., M. Hellmund 2015: Rare *in situ* preservation of adult crocodilian with eggs from the Middle Eocene of Geiseltal, Germany. – Palaios, 30, pp. 446–461.

Hayes, H.E. 2005: A partial double-layered eggshell in the tropical mockingbird (*Mimus gilvus*). – Ornitologia Neotropical, 16, pp. 263–266.

Hayward, J.L., K.F. Hirsch, T.C. Robertson 1991: Rapid dissolution of avian eggshells buried by Mount St. Helens ash. – Palaios, 6/2, pp. 174–178.

Hayward, J.L., D.K. Zelenitsky, D.L. Smith, D.M. Zaft, J.K. Clayburn 2000: Eggshell taphonomy at modern gull colonies and a dinosaur clutch site. – Palaios, 15/4, pp. 343–355.

Hayward, J.L., K.M. Dickson, S.R. Gamble, A.W. Owen, K.C. Owen 2011: Eggshell taphonomy: Environmental effects on fragment orientation. – Historical Biology, 23/1, pp. 5–13.

Hirsch, K.F. 1985: Fossil crocodilian eggs from the Eocene of Colorado. – Journal of Paleontology, 59, pp. 531–542.

Hirsch, K.F. 1989: Interpretations of Cretaceous and pre-Cretaceous eggs and shell fragments. – In: Gilette, D.D., M.G. Lockley (Eds): Dinosaur Tracks and Traces. Cambridge University Press, Cambridge, pp. 89–97.

Hirsch, K.F. 1996: Parataxonomic classification of fossil chelonian and gecko eggs. – Journal of Vertebrate Paleontology, 16, pp. 752–762.

Hirsch, K.F., J. Harris 1989: Fossil eggs from the lower Miocene Legetet formation of Koru, Kenya: Snail or lizard? – Historical Biology, 3, pp. 61–78.

Hirsch, K.F, B. Quinn 1990: Eggs and eggshell fragments from the Upper Cretaceous two medicine formation of Montana. – Journal of Vertebrate Paleontology, 10, pp. 491–511.

Hirsch, K.F., R. Kohring 1992: Crocodilian eggs from the middle Eocene Bridger formation, Wyoming. – Journal of Vertebrate Paleontology, 12, pp. 59–65.

Hirsch, K.F., L. Krishtalka, R.K. Stucky 1987: Revision of the Wind River faunas, Early Eocene of central Wyoming. Part 8. First fossil lizard egg (?Gekkonidae) and list of associated lizards. – Annals of Carnegie Museum, 56, pp. 223–230.

Horner, J.R. 1979: Upper Cretaceous dinosaurs from the Bearpaw Shale (marine) of south-central Montana with a checklist of Upper Cretaceous dinosaur remains from marine sediments in North America. – Journal of Paleontology, 53/3, pp. 566–577.

Horner, J.R. 1999: Egg clutches and embryos of two hadrosaurian dinosaurs. – Journal of Vertebrate Paleontology, 19, pp. 607–611.

Horner, J.R. 2000: Dinosaur reproduction and parenting. – Annual Review of Earth and Planetary Sciences, 28, pp. 19–45.

Hothorn, T., K. Hornik 2015: exactRankTests: Exact Distributions for Rank and Permutation Tests. – https://cran.r-project.org/web/packages/exactRankTests/index.html.

Hothorn, T., K. Hornik, M.A. van de Weil, H. Winell, A. Zeileis 2015: coin: Conditional Inference Procedures in a Permutation Test Framework. – https://cran.r-project.org/web/packages/coin/index.html.

Huh, M., S.B. Kim, Y. Woo, J.D. Simon, I.S. Paik, H.J. Kim 2014: First record of a complete giant theropod egg clutch from Upper Cretaceous deposits, South Korea. – Historical Biology, 26, pp. 218–228.

Jackson, F.D., D.J. Varricchio 2003: Abnormal, multilayered eggshell in birds: Implications for dinosaur reproductive anatomy. – Journal of Vertebrate Paleontology, 23, pp. 699–702.

Jackson, F.D., J.G. Schmitt 2008: Recognition of vertebrate egg abnormalities in the Upper Cretaceous fossil record. – Cretaceous Research, 29, pp. 27–39.

Jackson, F.D., D.J. Varricchio 2010: Fossil eggs and eggshell from the lowermost two medicine formation of Western Montana, Sevenmile hill locality. – Journal of Vertebrate Paleontology, 30, pp. 1142–1156.

Jackson, F.D., J.R. Horner, D.J. Varricchio 2010: A study of a *Troodon* egg containing embryonic remains using epifluorescence microscopy and other techniques. – Cretaceous Research, 31, pp. 255–262.

Jackson, F.D., J.G. Schmitt, S.E. Oser 2013: Influence of Vertisol development on sauropod egg taphonomy and distribution at the Auca Mahuevo locality, Patagonia, Argentina. – Palaeogeography, Palaeoclimatology, Palaeoecology, 386, pp. 300–307.

Jenkins, N.K. 1975: Chemical composition of the eggs of the crocodile (*Crocodylus novaeguineae*). – Comparative Biochemistry and Physiology, Part A: Physiology, 51, pp. 891–895.

Jin, X., Y. Azuma, F.D. Jackson, D.J. Varricchio 2007: Giant dinosaur eggs from the Tiantai basin, Zhejiang Province, China. – Canadian Journal of Earth Sciences, 44, pp. 81–88.

Jocha-Edelényi, E. 1988: History of evolution of the upper Cretaceous basin in the Bakony Mts at the time of the terrestrial Csehbánya Formation. – Acta Geologica Hungarica, 31, pp. 19–31.

Kerourio, P. 1981: La distribution des "coquilles d'oeufs de dinosauriens multistratiferiees" dans le Maestrichtien continental du sud de la France (Distribution of "multilayered dinosaurian eggshells" from the continental Maastrichtian of southern France). – Geobios, 14/4, pp. 533–536.

Kerourio, P. 1987: Présence d'oeufs de crocodiliens dans le Rognacien inférieur (Maastrichtien supérieur) du bassin d'Aix-en-Provence (Bouches-du-Rhône, France). Note préliminaire (Presence of crocodilian eggshells from the lower Rognacian (Upper Maastrichtian) of Aix-en-Provence basin (Bouches-du-Rhône, France). Preliminary note). – Geobios, 20, pp. 275–281.

Kidwell, S.M., K.W. Flessa 1996: The quality of the fossil record: Populations, species, and communities. – Annual Review of Earth and Planetary Sciences, 24, pp. 433–464.

Kocsis, L., A. Ősi, T. Vennemann, C.N. Trueman, M.R. Palmer 2009: Geochemical study of vertebrate fossils from the Upper Cretaceous (Santonian) Csehbánya Formation (Hungary): Evidence for a freshwater habitat of mosasaurs and pycnodont fish. – Palaeogeography, Palaeoclimatology, Palaeoecology, 280, pp. 532–542.

Kohring, R. 1991: Lizard egg shells from the lower Cretaceous of Cuenca Province, Spain. – Palaeontology, 34, pp. 237–240.

Kraus, M.J. 1999: Paleosols in clastic sedimentary rocks: Their geologic applications. – Earth-Science Reviews, 47/1, pp. 41–70.

Kundrát, M., A.R.I. Cruickshank, T.W. Manning, J. Nudds 2008: Embryos of therizinosauroid theropods from the Upper Cretaceous of China: Diagnosis and analysis of ossification patterns. – Acta Zoologica, 89, pp. 231–251.

Kurochkin, E.N., S. Chatterjee, K.E. Mikhailov 2013: An embryonic enantiornithine bird and associated eggs from the Cretaceous of Mongolia. – Paleontological Journal, 47, pp. 1252–1269.

Kusuda, S., Y. Yasukawa, H. Shibata, T. Saito, O. Doi, Y. Ohya, N. Yoshizaki 2013: Diversity in the matrix structure of eggshells in the Testudines (Reptilia). – Zoological Science, 30, pp. 366–374.

Lauters, P., Y.L. Bolotsky, J. Van Itterbeeck, P. Godefroit 2008: Taphonomy and age profile of a latest Cretaceous dinosaur bone bed in Far Eastern Russia. – Palaios, 23/3, pp. 153–162.

Lee, Y.N. 1996: A new nodosaurid ankylosaur (Dinosauria: Ornithischia) from the Paw Paw Formation (late Albian) of Texas. – Journal of Vertebrate Paleontology, 16/2, pp. 232–245.

Li, N., L.N. Niu, Y.P. Qi, C.K.Y. Yiu, H. Ryou, D.D. Arola, J.H. Chen, D.H. Pashley, F.R. Tay 2011: Subtleties of biomineralisation revealed by manipulation of the eggshell membrane. – Biomaterials, 32/34, pp. 8743–8752.

Liang, X., S. Wen, D. Yang, S. Zhou, S. Wu 2009: Dinosaur eggs and dinosaur egg-bearing deposits (Upper Cretaceous) of Henan Province, China: Occurrences, palaeoenvironments, taphonomy and preservation. – Progress in Natural Science, 19/11, pp. 1587–1601.

López-Martínez, N. 2003: Dating dinosaur oodiversity: Chronostratigraphic control of Late Cretaceous oospecies succession. – Palaeovertebrata, 32, pp. 121–148.

López-Martínez, N., E. Vicens 2012: A new peculiar dinosaur egg, *Sankofa pyrenaica* oogen. nov. oosp. nov. from the Upper Cretaceous coastal deposits of the Aren Formation, south-central Pyrenees, Lleida, Catalonia, Spain. – Palaeontology, 55, pp. 325–339.

López-Martinez, N., J.J. Moratalla, J.L. Sanz 2000: Dinosaurs nesting on tidal flats. – Palaeogeography, Palaeoclimatology, Palaeoecology, 160, pp. 153–163.

López-Martínez, N., J.I. Canudo, L. Ardèvol, X. Pereda Superbiola, X. Oure-Etxebarria, G. Cuenca-Bescós, J.I. Ruiz-Omeñaca, X. Murelaga, M. Feist 2001: New dinosaur sites correlated with Upper Maastrichtian pelagic deposits in the Spanish Pyrenees: Implications for the dinosaur extinction pattern in Europe. – Cretaceous Research, 22, pp. 41–61.

Mackenzie, F.T. 2014: Sediments, Diagenesis, and Sedimentary Rocks: Treatise on Geochemistry (2nd ed.). – Elsevier, Amsterdam, 656 p.

Makádi, L. 2006: *Bicuspidon* aff. *hatzegiensis* (Squamata: Scincomorpha: Teiidae) from the Upper Cretaceous Csehbánya Formation (Hungary, Bakony Mts). – Acta Geologica Hungarica, 49, pp. 373–385.

Makádi, L. 2013a: The first known chamopsiid lizard (Squamata) from the Upper Cretaceous of Europe (Csehbánya Formation; Hungary, Bakony Mts). – Annales de Paléontologie, 99, pp. 261–274.

Makádi, L. 2013b: A new polyglyphanodontine lizard (Squamata: Borioteiioidea) from the Late Cretaceous Iharkút locality (Santonian, Hungary). – Cretaceous Research, 46, pp. 166–176.

Makádi, L., R.L. Nydam 2015: A new durophagous scincomorphan lizard genus from the Late Cretaceous Iharkút locality (Hungary, Bakony Mts). – Paläontologische Zeitschrift, 89, pp. 925–941.

Makádi, L., M.W. Caldwell, A. Ősi 2012: The first freshwater mosasauroid (Upper Cretaceous, Hungary) and a new clade of basal mosasauroids. – PLoS One, 7/12, p. e51781.

Makovicky, P.J., G. Grellet-Tinner 2000: Association between theropod eggshell and a specimen of *Deinonychus antirrhopus*. – In: Bravo, A., T. Reyes (Eds): First International Symposium on Dinosaur Eggs and Babies. Extended Abstracts. Publicacions de la Diputacio' de Lleida, Lleida, pp. 123–128.

Marzola, M., J. Russo, O. Mateus 2015: Identification and comparison of modern and fossil crocodilian eggs and eggshell structures. – Historical Biology, 27, pp. 115–133.

Mateus, I., H. Mateus, M. Telles Antunes, O. Mateus, P. Taquet, V. Riberio, G. Manuppella 1997: Couvée, œufs et embryons d'un Dinosaure Théropode du Jurassique supérieur de Lourinhã (Portugal) (Nest, eggs and embryos of a theropod dinosaur from the Upper Jurassic of Lourinhã (Portugal)) . – Comptes Rendus del'Académie des Sciences, Series IIA: Earth and Planetary Sciences, 325, pp. 71–78.

McCrea, R.T., M.G. Lockley, C.A. Meyer 2001: Global distribution of purported ankylosaur track occurrence. – In: Carpenter, K. (Ed): The Armored Dinosaurs. Indiana University Press, Bloomington, pp. 413–454.

Mikhailov, K.E. 1991: Classification of fossil eggshells of amniotic vertebrates. – Acta Paleontologica Polonica, 36, pp. 193–238.

Mikhailov, K.E. 1997: Fossil and recent eggshell in amniotic vertebrates: Fine structure, comparative morphology and classification. – Special Papers in Palaeontology, 56, pp. 1–80.

Minchin, P.R., J. Oksanen 2015: Global and Local Non-metric Multidimensional Scaling and Linear and Hybrid Scaling. – http://artax.karlin.mff.cuni.cz/r-help/library/vegan/html/monoMDS.html.

Mindszenty, A., A. Csoma, Á. Török, K. Hips, E. Hertelendi 2000: Rudistid limestones, bauxites, paleokarst and geodynamics. The case of the Cretaceous of the Transdanubian Range. – Földtani Közlöny, 131, pp. 107–152.

Moore, J.R., D.B. Norman 2009: Quantitatively evaluating the sources of taphonomic biasing of skeletal element abundances in fossil assemblages. – Palaios, 24, pp. 591–602.

Moreno-Azanza, M., B. Bauluz, J.I. Canudo, E. Puértolas-Pascual, A.G. Sellés 2014: A re-evaluation of aff. Megaloolithidae eggshell fragments from the uppermost Cretaceous of the Pyrenees and implications for crocodylomorph eggshell structure. – Historical Biology, 26, pp. 195–205.

Moreno-Azanza, M., B. Bauluz, J.I. Canudo, J.M. Gasca, F.T. Fernández-Baldor 2016: Combined use of electron and light microscopy techniques reveals false secondary shell units in Megaloolithidae eggshells. – PLoS One, 11/5, p. e0153026.

Norell, M.A., J.M. Clark, D. Dashzeveg, T. Barsbold, L.M. Chiappe, A.R. Davidson, M.C. McKenna, P. Altangerel, M.J. Novacek 1994: A theropod dinosaur embryo, and the affinities of the Flaming Cliffs Dinosaur eggs. – Science, 266, pp. 779–782.

Novas, F.E., D.F. Pais, D. Pol, I.D.S. Carvalho, A. Scanferla, A. Mones, M. Suárez Riglos 2009: Bizarre notosuchian crocodyliform with associated eggs from the Upper Cretaceous of Bolivia. – Journal of Vertebrate Paleontology, 29/4, pp. 1316–1320.

Oser, S.E., F.D. Jackson 2014: Sediment and eggshell interactions: Using abrasion to assess transport in fossil eggshell accumulations. – Historical Biology, 26/2, 165–172.

Ősi, A. 2005: *Hungarosaurus tormai*, a new ankylosaur (Dinosauria) from the Upper Cretaceous of Hungary. – Journal of Vertebrate Paleontology, 25/2, pp. 370–383.

Ősi, A. 2008: Enantiornithine bird remains from the Late Cretaceous of Hungary. – Oryctos, 7, pp. 55–60.

Ősi, A., L. Makádi 2009: New remains of *Hungarosaurus tormai* (Ankylosauria, Dinosauria) from the Upper Cretaceous of Hungary: Skeletal reconstruction and body mass estimation. – Paläontologische Zeitschrift, 83, pp. 227–245.

Ősi, A., E. Prondvai 2013: Sympatry of two ankylosaurs (*Hungarosaurus* and cf. *Struthiosaurus*) in the Santonian of Hungary. – Cretaceous Research, 44, pp. 58–63.

Ősi, A., J.M. Clark, D.B. Weishampel 2007: First report on a new basal eusuchian crocodyliform with multicusped teeth from the Upper Cretaceous (Santonian) of Hungary. – Neues Jahrbuch für Geologie und Palaontologie, 243, pp. 169–177.

Ősi, A., R.J. Butler, D.B. Weishampel 2010a: A Late Cretaceous ceratopsian dinosaur from Europe with Asian affinities. – Nature, 465, pp. 466–468.

Ősi, A., S.M. Apesteguía, M. Kowalewski 2010b: Non-avian theropod dinosaurs from the early Late Cretaceous of Central Europe. – Cretaceous Research, 31, pp. 304–320.

Ősi, A., L. Makádi, M. Rabi, Z. Szentesi, G. Botfalvai, P. Gulyás 2012a: The late Cretaceous continental vertebrate fauna from Iharkút, western Hungary: A review. – In: Godefroit, P. (Ed): Bernissart Dinosaurs and Early Cretaceous Terrestrial Ecosystems. Indiana University Press, Bloomington, pp. 532–569.

Ősi, A., E. Prondvai, R. Butler, D.B. Weishampel 2012b: Phylogeny, histology and inferred body size evolution in a new rhabdodontid dinosaur from the Late Cretaceous of Hungary. – PLoS One, 7/9, p. e44318.

Österström, O., L. Holm, C. Lilja 2013: Calcium mobilization from the avian eggshell during embryonic development. – Animal Biology, 63, pp. 33–46.

Packard, M.J., K.F. Hirsch 1989: Structure of shells from eggs of the geckos *Gekko gecko* and *Phelsuma madagascarensis*. – Canadian Journal of Zoology, 67, pp. 746–758.

Packard, M.J., V.G. Demarco 1991: Eggshell structure and formation in eggs of oviparous reptiles. – In: Deeming, C.D., M.W.J. Ferguson (Eds): Egg Incubation: Its Effects on Embryonic Development in Birds and Reptiles. Cambridge University Press, Cambridge, pp. 53–70.

Paik, I.S., M. Huh, H.J. Kim 2004: Dinosaur egg-bearing deposits (Upper Cretaceous) of Boseong, Korea: Occurrence, palaeoenvironments, taphonomy, and preservation. – Palaeogeography, Palaeoclimatology, Palaeoecology, 205/1, pp. 155–168.

Patnaik, R., A. Sahni, D. Cameron, B. Pillans, P. Chatrath, E. Simons, M. Williams, F. Bibi 2009: Ostrich-like eggshells from a 10.1 million-yr-old Miocene ape locality, Haritalyangar, Himachal Pradesh, India. – Current Science, 96, pp. 1485–1495.

Pereda-Suberbiola, X. 1992: A revised census of European Late Cretaceous nodosaurids (Ornithischia: Ankylosauria): Last occurrence and possible extinction scenarios. – Terra Nova, 4, pp. 641–648.

Pike, D.A., R.M. Andrews, W.G. Du 2012: Eggshell morphology and gekkotan life-history evolution. – Evolutionary Ecology, 26, pp. 847–861.

Rabi, M., N. Sebők 2015: A revised Eurogondwana model: Late Cretaceous notosuchian crocodyliforms and other vertebrate taxa suggest the retention of episodic faunal links between Europe and Gondwana during most of the Cretaceous. – Gondwana Research, 28/3, pp. 1197–1211.

Rabi, M., H. Tong, G. Botfalvai 2011: A new species of the side-necked turtle *Foxemys* (Pelomedusoides: Bothremydidae) from the Late Cretaceous of Hungary and the historical biogeography of the Bothremydini. – Geological Magazine, 149, pp. 662–674.

Retallack, G.J. 1984: Completeness of the rock and fossil record: Some estimates using fossil soils. – Paleobiology, 10/1, pp. 59–78.

Retallack, G.J. 2001: Soils of the Past: An Introduction to Paleopedology (2nd ed.). – Blackwell Publishing, Oxford, 404 p.

Riberio, V., O. Mateus, F. Holwerda, R. Araújo, R. Castanhinha 2013: Two new theropod egg sites from the Late Jurassic Lourinhã Formation, Portugal. – Historical Biology, 26, pp. 206–217.

Riley, A., C.J. Sturrock, S.J. Mooney, M.R. Luck 2014: Quantification of eggshell microstructure using X-ray micro computed tomography. – British Poultry Science, 55/3, pp. 311–320.

Roberts, E.M. 2007: Facies architecture and depositional environments of the Upper Cretaceous Kaiparowits Formation, southern Utah. – Sedimentary Geology, 197/3, pp. 207–233.

Sabath, K. 1991: Upper Cretaceous amniotic eggs from the Gobi desert. – Acta Palaeontologica Polonica, 36, pp. 151–192.

Sander, P.M., A. Christian, M. Clauss, R. Fechner, C.T. Gee, E.M. Griebeler, H.C. Gunga, J. Hummel, H. Mallison, S.F. Perry, H. Preuschoft, O.W.M. Rauhut, K. Remes, T. Tütken, O. Wings, U. Witzel 2011: Biology of the sauropod dinosaurs: The evolution of gigantism. – Biological Reviews, 86, pp. 117–155.

Schweitzer, M.H., F.D. Jackson, L.M. Chiappe, J.G. Schmitt, J.O. Calvo, D.E. Rubilar 2002: Late Cretaceous avian eggs with embryos from Argentina. – Journal of Vertebrate Paleontology, 22, pp. 191–195.

Sellés, A.G., B. Vila 2015: Re-evaluation of the age of some dinosaur localities from the southern Pyrenees by means of megaloolithid oospecies. – Journal of Iberian Geology, 41/1, pp. 125–139.

Sellés, A.G, À. Galobart 2016: Reassessing the endemic European Upper Cretaceous dinosaur egg *Cairanoolithus*. – Historical Biology, 28/5, pp. 538–596.

Sellés, A.G., A.M. Bravo, X. Delclòs, F. Colombo, X. Martí, J. Ortega-Blanco, C. Parellada, À. Galobart 2013: Dinosaur eggs in the Upper Cretaceous of the Coll de Nargó area, Lleida Province, south-central Pyrenees, Spain: Oodiversity, biostratigraphy and their implications. – Cretaceous Research, 40, pp. 10–20.

Sellés, A.G., B. Vila, À. Galobart 2014: Diversity of theropod ootaxa and its implications for the latest Cretaceous dinosaur turnover in southwestern Europe. – Cretaceous Research, 49, pp. 45–54.

Smith, D.L., J.L. Hayward 2010: Bacterial decomposition of avian eggshell: A taphonomic experiment. – Palaios, 25, pp. 318–326.

Suzuki, R., H. Shimodaira 2014: Hierarchical Clustering with P-Values via Multiscale Bootstrap Resampling. – https://cran.r-project.org/web/packages/pvclust/index.html.

Tanaka, K., D.K. Zelenitsky, T. Williamson, A. Weil, F. Therrien 2011: Fossil eggshells from the Upper Cretaceous (Campanian) fruitland formation, New Mexico. – Historical Biology, 23, pp. 41–55.

Tanaka, K., D.K. Zelenitsky, F. Therrien 2015: Eggshell porosity provides insight on evolution of nesting in dinosaurs. – PLoS One, 10/11, p. e0142829.

Tari, G. 1994: Alpine tectonics of the Pannonian Basin. – Ph.D. Thesis, Rice University, Houston, 501 p.

Therrien, F. 2005: Palaeoenvironments of the latest Cretaceous (Maastrichtian) dinosaurs of Romania: Insights from fluvial deposits and paleosols of the Transylvanian and Haţeg basins. – Palaeogeography, Palaeoclimatology, Palaeoecology, 218/1, pp. 15–56.

Tribovillard, N., P. Récourt, A. Trentesaux 2010: Bacterial calcification as a possible trigger for francolite precipitation under sulfidic conditions. – Comptes Rendus Geoscience, 342/1, pp. 27–35.

Trueman, C.N., N. Tuross 2002: Trace elements in recent and fossil bone apatite. – Reviews in Mineralogy and Geochemistry, 48, pp. 489–521.

Tucker, M.E., V.P. Wright 1990: Carbonate Sedimentology. – Blackwell Publishing, Oxford, 482 p.

Tyler, C., S. Fowler 1978: The distribution of organic cores, cones, cone junctions and pores in the egg shells of wild birds. – Journal of Zoology, 186, pp. 1–14.

Van Itterbeeck, J., E. Sasaran, V. Codrea, L. Sasaran, P. Bultynck 2004: Sedimentology of the Upper Cretaceous mammal- and dinosaur-bearing sites along the Râul Mare and Barbat rivers, Hateg Basin, Romania. – Cretaceous Research, 25/4, pp. 517–530.

Varricchio, D.J., F.D. Jackson 2004: A phylogenetic assessment of prismatic dinosaur eggs from the Cretaceous two medicine formation of Montana. – Journal of Vertebrate Paleontology, 24, pp. 931–937.

Varricchio, D.J., J.R. Horner, F.D. Jackson 2002: Embryos and eggs for the Cretaceous theropod dinosaur *Troodon formosus*. – Journal of Vertebrate Paleontology, 22, pp. 564–576.

Varricchio, D.J., F.D. Jackson, R.A. Jackson, D.K. Zelenitsky 2013: Porosity and water vapor conductance of two *Troodon formosus* eggs: An assessment of incubation strategy in a maniraptorandinosaur. – Paleobiology, 39, pp. 278–296.

Vasile, S., Z. Csiki 2011: New Maastrichtian microvertebrates from the Rusca Montană Basin (Romania). – Muzeul Olteniei Craiova, 27, pp. 221–230.

Venczel, M., S. Vasile, Z. Csiki-Sava 2015: A Late Cretaceous madtsoiid snake from Romaina associated with a megaloolithid egg nest – Paleoecological inferences. – Cretaceous Research, 55, pp. 152–163.

Vianey-Liaud, M., N. López-Martínez 1997: Late Cretaceous dinosaur eggshells from the Tremp Basin, Southern Pyrenees, Lleida, Spain. – Journal of Vertebrate Paleontology, 71, pp. 1157–1171.

Vianey-Liaud, M., A. Khosla, G. Garcia 2003: Relationships between European and Indian dinosaur eggs and eggshells of the oofamily Megaoolithidae. – Journal of Vertebrate Paleontology, 23/3, pp. 575–585.

Vila, B., V. Riera, A.M. Bravo, O. Oms, E. Vicens, R. Estrada, À. Galobart 2011: The chronology of dinosaur oospecies in south-western Europe: Refinements from the Maastrichtian succession of the eastern Pyrenees. – Cretaceous Research, 32, pp. 378–386.

Weishampel, D.B., D.E. Fastovsky, M. Watabe, D. Varricchio, F. Jackson, K. Tsogtbaatar, R. Barsbold 2008: New oviraptorid embryos from Bugin-Tsav, Nemegt Formation (Upper Cretaceous), Mongolia, with insights into their habitat and growth. – Journal of Vertebrate Paleontology, 28, pp. 1110–1119.

Williams, D.L.G., R.S. Seymour, P. Kerourio 1984: Structure of fossil dinosaur eggshell from the Aix Basin, France. – Palaeogeography, Palaeoclimatology, Palaeoecology, 45, pp. 23–37.

Wink, C.S., R.M. Elsey 1994: Morphology of shells from viable and nonviable eggs of the Chinese alligator (*Alligator sinensis*). – Journal of Morphology, 222, pp. 103–110.

Wink, C.S., R.M. Elsey, M. Bouvier 1990: The relationship of pores and mammillae on the inner surface of the eggshell of the alligator (*Alligator mississippiensis*). – Journal of Morphology, 204, pp. 227–233.

Witt, L.J., J.P. Caldwell 2004: Herpetology: An Introductory Biology of Amphibians and Reptiles (3rd ed.). – Elsevier Academic Press, Cambridge, 697 p.

Zeigler, K.E. 2005: Taphonomic analysis of a fire-related Upper Triassic vertebrate fossil assemblage from North-Central New Mexico. – Geology of the Chama Basin. New Mexico Geological Society, 56th Field Conference Guidebook, pp. 341–354.

Zelenitsky, D.K., L.V. Hills 1997: Normal and pathological eggshells of *Spheroolithus albertensis*, oosp. nov., from the Oldman Formation (Judith River Group, late Campanian), southern Alberta. – Journal of Vertebrate Paleontology, 17, pp. 167–171.

Zelenitsky, D.K., K.F. Hirsch 1997: Fossil eggs: Identification and classification. – In: Wolberg, D.L., E. Stump, G.D. Rosenberg (Eds): Dinofest International. Academy of Natural Sciences, Philadelphia, pp. 279–286.

Zelenitsky, D.K., S.P. Modesto 2003: New information on the eggshell of ratites (Aves) and its phylogenetic implications. – Canadian Journal of Zoology, 81, pp. 962–970.

Zelenitsky, D.K., L.V. Hills, P.J. Currie 1996: Parataxonomic classification of ornithoid eggshell fragments from the Oldman Formation (Judith River Group; Upper Cretaceous), southern Alberta. – Canadian Journal of Earth Sciences, 33, pp. 1655–1667.

Zelenitsky, D.K, K. Carpenter, P.J. Currie 2000: First record of elongatoolithid theropod eggshell from North America: The Asian oogenus *Macroelongatoolithus* from the lower Cretaceous of Utah. – Journal of Vertebrate Paleontology, 20, pp. 130–138.

Zhang, Y., Y. Liu, X. Ji, C.E. Banks, J. Song 2011: Flower-like agglomerates of hydroxyapatite crystals formed on an egg-shell membrane. – Colloids and Surfaces B, 82/2, pp. 490–496.

Zhang, S., X. Jin, J. O'Connor, M. Wang, J. Xie 2015: A new egg with avian egg shape from the Upper Cretaceous of Zhejiang Province, China. – Historical Biology, 27/5, pp. 595–602.